Molecular Biology of the Cell
Vol. 7, 803–823, May 1996

Re-expression of ABP-120 Rescues Cytoskeletal, Motility, and Phagocytosis Defects of ABP-120$^-$ *Dictyostelium* Mutants

Dianne Cox,*† Deborah Wessels,‡ David R Soll,‡ John Hartwig,§ and John Condeelis*¶

*Department of Anatomy and Structural Biology, Albert Einstein College of Medicine, Bronx, New York 10461; ‡University of Iowa, Iowa City, Iowa 52242; and §Brigham and Women's Hospital, Harvard Medical School, Boston, Massachusetts 02134

Submitted October 13, 1995; Accepted February 28, 1996
Monitoring Editor: Thomas D. Pollard

The actin binding protein ABP-120 has been proposed to cross-link actin filaments in nascent pseudopods, in a step required for normal pseudopod extension in motile *Dictyostelium* amoebae. To test this hypothesis, cell lines that lack ABP-120 were created independently either by chemical mutagenesis or homologous recombination. Different phenotypes were reported in these two studies. The chemical mutant shows only a subtle defect in actin cross-linking, while the homologous recombinant mutants show profound defects in actin cross-linking, cytoskeletal structure, pseudopod number and size, cell motility and chemotaxis and, as shown here, phagocytosis. To resolve the controversy as to what the ABP-120$^-$ phenotype is, ABP-120 was re-expressed in an ABP-120$^-$ cell line created by homologous recombination. Two independently "rescued" cell lines that express wild-type levels of ABP-120 were analyzed. In both rescued cell lines, actin incorporation into the cytoskeleton, pseudopod formation, cell morphology, instantaneous velocity, phagocytosis, and chemotaxis were restored to wild-type levels. There is no alteration in the expression levels of several related actin binding proteins in either the original ABP-120$^-$ cell line or in the rescued cell lines, leading to the conclusion that neither the aberrant phenotype observed in ABP-120$^-$ cells nor the normal phenotype reasserted in rescued cells can be attributed to alterations in the levels of other abundant and related actin binding proteins. Re-expression of ABP-120 in ABP-120$^-$ cells reestablishes normal structural and behavioral parameters, demonstrating that the severity and properties of the structural and behavioral defects of ABP-120$^-$ cell lines produced by homologous recombination are the direct result of the absence of ABP-120.

INTRODUCTION

Pseudopod extension is the basis of cellular locomotion in amoeboid cells and plays a critical role in chemotaxis (Zigmond, 1977; Condeelis *et al.*, 1993a; Soll, 1995). Extension of a localized pseudopod is the first locomotive step when a cell is challenged with a focal source of a chemoattractant, as seen in *Dictyostelium* (Gerisch *et al.*, 1975) and leukocytes (Zigmond and Sullivan, 1979; Stephans and Synderman, 1982). Several models have been proposed to account for polarized pseudopod extension, such as the "Tail Contraction Model" (Mast, 1926), the "Frontal Sliding Model" (Sheetz *et al.*, 1992), and the "Cortical Expansion Model" (Condeelis *et al.*, 1993b). The "Cortical Expansion Model" predicts that the cross-linking of actin filaments, but not myosin-mediated sliding, is essential for pseudopod formation. The actin binding

† The data in this paper are from a thesis to be submitted in partial fulfillment of the requirements for the Degree of Doctor of Philosophy in the Sue Golding Graduate Division of Medical Sciences, Albert Einstein College of Medicine, Yeshiva University.

¶ Corresponding author.

protein in *Dictyostelium* that is most likely to fulfill this cross-linking function is ABP-120.

ABP-120 is a dimer consisting of two identical subunits each with a molecular weight of 120,000 on SDS-PAGE (Condeelis *et al.*, 1984), which are packed in an anti-parallel orientation (Brink *et al.*, 1990). Based on structural similarities, ABP-120 has been proposed to be a member of the filamin family of actin binding proteins, which is composed of ABP, ABP-280, and nonmuscle filamin (Hartwig and Kwiatkowski, 1991; Matsudaira, 1991).

Members of this family of actin binding proteins have been implicated in pseudopod extension. Immunofluorescence analysis demonstrates that both ABP and ABP-120 are concentrated in the cell cortex, in lamellipods, and in pseudopods during cell spreading and locomotion (Stendahl *et al.*, 1980; Condeelis *et al.*, 1981; Carboni and Condeelis, 1985). In the case of ABP-120, preferential localization in pseudopods has been demonstrated after cAMP stimulation (Condeelis *et al.*, 1988). In addition, ABP-120 becomes incorporated into the actin cytoskeleton at times after stimulation with cAMP that correlate with cross-linking of actin into the cytoskeleton and with pseudopod extension (Hall *et al.*, 1988; Dharmawardhane *et al.*, 1989). ABP and ABP-120 cross-link actin filaments in vitro to form a rigid actin gel containing orthogonal networks similar to those observed in pseudopods in situ (Condeelis *et al.*, 1984; Hartwig and Shevlin, 1986; Wolosewick and Condeelis, 1986; Ogihara *et al.*, 1988). Both proteins have also been localized to filament networks found in pseudopods in situ by immunoelectron microscopy (Hartwig and Shevlin, 1986; Ogihara *et al.*, 1988; Cox *et al.*, 1995).

Pseudopods formed in response to a phagocytic signal are very similar to the ones produced in response to a chemotactic signal. The kinetics of actin polymerization in macrophages during phagocytosis (Greenberg *et al.*, 1991) are similar to those observed in neutrophils during chemotactic stimulation (Howard and Oresajo, 1985; Harvath, 1990). The morphological fine structure of pseudopods formed in response to both phagocytic and chemotactic signals are similar for both macrophages and *Dictyostelium* (Reaven and Axline, 1973; Hartwig and Shevlin, 1986; Fukui *et al.*, 1989; Cox *et al.*, 1995). It follows from these observations that pseudopods formed during both types of processes are likely to be generated by the same mechanism involving the same cytoskeletal proteins.

Two groups have independently deleted ABP-120 expression in *Dictyostelium* amoebae, but have obtained differing results. One group first created an ABP-120$^-$ cell line by chemical mutagenesis and found a subtle phenotype in actin filament cross-linking (Brink *et al.*, 1990). This same group created a double mutant by deletion of both ABP-120 and α-actinin. In the double mutant development was greatly impaired. When α-actinin was re-expressed in the double mutant the developmental defect was rescued (Witke *et al.*, 1992).

The second group created ABP-120$^-$ cell lines by homologous recombination. Deletion of ABP-120 in two independent strains of *Dictyostelium* resulted in profound changes in the biochemical and structural properties of mutant cells including decreased actin cross-linking in the cytoskeleton, reduction in the size and frequency of pseudopods, dramatic alterations in the organization of filament networks in pseudopods, reduction in translocation velocity, and a reduction in chemotactic efficiency when compared with ABP-120$^+$ control cell lines (Cox *et al.*, 1992, 1995). The defect in pseudopod extension correlated with changes in filament cross-linking in pseudopods as shown by biochemical and electron microscopic analysis (Cox *et al.*, 1995).

Restoring the mutant to a wild-type phenotype by re-expression of the protein results in definitive proof that a phenotype observed in a mutant cell line is due specifically to the deleted protein. In this study we have examined whether the defects in cross-linking, pseudopod formation, motility, and chemotaxis exhibited by ABP-120$^-$ cells are due specifically to the deletion of ABP-120 by re-expression of ABP-120 in a formerly ABP-120$^-$ cell line. In addition, we have studied the relationship between pseudopod extension and phagocytosis in ABP-120$^-$ mutants and rescued cell lines to determine whether defects in pseudopod properties in ABP-120$^-$ cells directly caused defects in phagocytosis.

MATERIALS AND METHODS

Transformation Vectors

Two different vectors were used that contain the PYR5–6 coding sequence, pUCPYR5–6 containing the entire coding region of the PYR5–6 gene and g7PYR5Δ6.2 in which the *Pvu*II/*Hin*cII fragment of the coding region has been removed. Both vectors were generous gifts from David Knecht, University of Connecticut, Storrs, CT. To construct the ABP-120 re-expression vector, the entire coding region of ABP-120 was isolated from a λgt11 clone after partial *Eco*RI digestion and then subcloned into the *Eco*RI site of pBluescript II. A *Xba*I/*Hae*III fragment of the actin 15 promotor from pDNEO II (Witke *et al.*, 1987) was subcloned into the *Xba*I/*Sma*I sites of the vector 5′ to the ABP-120 coding region. A *Hin*dIII fragment containing the actin 8 terminator was placed in the *Hin*dIII site 3′ to the ABP-120 stop codon. For integration into the PYR5–6 locus, the *Pvu*II/*Hin*cII fragment of the PYR5–6 coding region was subcloned into the *Sac*II site of the vector. The resulting transformation vector is pABP-120PYR.

Transformation

Dictyostelium amoebae were transformed by electroporation according to the method of Dynes and Firtel (1989) except the curing phase was omitted. For selection of ura$^-$ cells, transformants were selected in final minimal medium (Franke and Kessin, 1977) that contained 100 μg/ml uracil and 100 μg/ml 5-fluoro-orotic acid. Ura$^+$ transformants were selected in final minimal medium alone (Kalpaxis *et al.*, 1990).

Southern Blots

DNA was prepared using a DNA miniprep procedure (Knecht *et al.*, 1990). DNA was digested with restriction enzymes as indicated, electrophoresed on 0.5% Sea-Kem agarose (FMC, Rockland, ME), and transferred to Hybond-N+ nylon membrane (Amersham Life Sciences, Arlington Heights, IL). Southern blots were hybridized with a randomly primed labeled probe of the entire ABP-120 coding region and developed using the enhanced chemoluminescence protocol (Amersham Life Sciences).

Growth Conditions

The cells were basically handled according to the method of Hall *et al.* (1988). Cells were routinely grown in HL5 medium with or without the addition of 10 μg/ml G418 depending on the drug resistance of each cell line.

For growth in bacterial suspensions each lawn of *Klebsiella aerogenes* (KA), which was grown overnight on a SM agar plate, was resuspended in 40 ml of 14.8 mM NaH_2PO_4, 5.2 mM K_2HPO_4, pH 6.6 (20 mM Na/K/PO_4 buffer). This bacterial suspension was aliquoted into separate flasks and inoculated with the various *Dictyostelium* cell lines at an initial density of approximately 1×10^5 cells/ml. This suspension was shaken at 21°C, 175 rpm. *Dictyostelium* cell growth was monitored over time by counting cells using a hemocytometer. The clearance of bacteria from the same suspension was monitored by removing an aliquot of the suspension, pelleting the *Dictyostelium* cells by a gentle centrifugation that pellets only the *Dictyostelium* cells and not the bacteria (4 min, 185 $\times$ *g*), and measuring the absorbance at OD_{600} of the bacteria remaining in suspension. As a control, a bacterial suspension without added *Dictyostelium* cells was monitored over the same period of time. The density of this control suspension did not change, indicating that over the course of the experiment there was no bacterial cell growth or death.

To analyze colony morphology, a toothpick was dipped into a suspension of cells grown in HL5 and then the tip was touched in the middle of a pre-grown KA lawn. The plates were incubated at 21°C and the growth of the colony monitored over time. Colony diameter was measured in two different directions and then averaged. For the clear zone width, two different areas were measured and then averaged.

Analysis of Phagocytosis

Phagocytosis assays were done according to the method Cohen *et al.* (1994) with minor modifications.

Fluorescent Labeling of Bacteria: Bacteria were grown in Luria-Bertani medium to a density of $OD_{600} = 2$. The bacteria were pelleted and resuspended in 0.1 volume of 50 mM Na_2HPO_4, pH 9.2, containing 0.1 mg/ml fluorescein isothiocyanate (Sigma, St. Louis, MO). The mixture was shaken at 150 rpm for 1 h at 30°C and the bacteria were then washed by repeated centrifugation in Sorenson's buffer until all unreacted fluorescence was removed. The bacteria were then resuspended to 2.5×10^{10} in Sorenson's buffer.

Quantitation of Bacterial Uptake: Dictyostelium cells that were growing exponentially in HL5 were washed once with Sorenson's buffer and then resuspended to a density of 2×10^6 cells/ml in Sorenson's buffer containing 5×10^9 bacteria/ml. The cells were shaken at 150 rpm at 21°C. Uptake was stopped at various times by diluting an aliquot of the cell mixture in 9 volumes of ice cold Sorenson's buffer. The *Dictyostelium* cells in the samples were pelleted by centrifugation at 185 $\times$ *g* for 4 min. The cells were then washed three times with Sorenson's buffer containing 2 mM EDTA to remove the majority of uningested bacteria. After the last wash, cells were resuspended to an approximate density of 2×10^6 cells/ml in 50 mM Na_2HPO_4 buffer, pH 9.2. The cells were counted and then lysed by the addition of 0.2% Triton X-100. The fluorescence was measured with a Hitachi F-2000 spectrofluorimeter using excitation and emission wavelengths of 490 and 520 nm, respectively. To determine the total number of bacteria ingested, this value was compared with a standard curve generated by lysing defined numbers of bacteria in 50 mM Na_2HPO_4 buffer, pH 9.2, containing 1% SDS.

Pinocytosis Assay

The pinocytosis assay was performed basically according to the method of Cohen *et al.* (1994). Cells grown in HL5 were harvested, washed, and resuspended to a final density of 4×10^6 cells/ml in Sorenson's buffer. Fluorescein isothiocyanate-dextran (2 mg/ml; Sigma) was added and the cells were incubated at 21°C in shaking suspension for various times. To stop the assay, the cells were diluted 10-fold in ice-cold Sorenson's buffer. To remove the uningested dextran, the cells were washed three times with Sorenson's buffer containing 2 mM EDTA. After the last wash, cells were resuspended to an approximate density of 2×10^6 cells/ml in 50 mM Na_2HPO_4 buffer, pH 9.2. The cells were counted and then lysed by the addition of 0.2% Triton X-100. The fluorescence was measured with an Hitachi F-2000 spectrofluorimeter as described.

Protein Quantitation

To prepare whole cell lysates, cells were grown to mid-log phase in HL5 medium and either harvested or starved for 6 h in a solution containing 14.8 mM NaH_2PO_4 and 5.2 mM K_2PO_4, pH 6.6 (20 mM Na/K/PO_4), and then harvested. Harvested cells were washed in 20 mM Na/K/PO_4 and then resuspended to a final density of 2×10^6 cells/ml in ice-cold 20 mM Na/K/PO_4 containing 2 mM EDTA, 2 mM EGTA, 0.04 ml/ml aprotinin, and 20 μg/ml each of chymostatin and leupeptin (Sigma). An equal volume of 2$\times$ Laemmli sample buffer was added, and the samples were vortexed for 10 s and heated to 100°C for 5 min. Samples were immediately loaded (2.5 μl/well) and run on either 8% or 10% SDS-PAGE gels. The gels were subsequently Western blotted or stained with Coomassie brilliant blue. The levels of actin, myosin, and ABP-240 were determined from Coomassie-stained gels. The intensity of the specific band (actin, 42 kDa; myosin II, 200 kDa; and ABP-240, 240 kDa), as determined by scanning densitometry (Molecular Dynamics, Sunnyvale, CA), was divided by the total intensity of the whole cell lane to obtain the percent total protein.

For Western blots, SDS-PAGE gels were transferred onto 0.2-μm nitrocellulose filters (Scheicher & Schuell, Keene, NH) by the use of a semi-dry blotter (Bio-Rad, Richmond, CA) at 20 volts for 1 h. These conditions insured quantitative transfer of most proteins below 200 kDa. The filters were incubated in either 0.05 μg/ml affinity-purified polyclonal anti-ABP-120 or 0.1 μg/ml affinity-purified polyclonal anti-α-actinin. Both antibodies have been shown to be monospecific (Carboni and Condeelis, 1985). The Western blots were developed using the enhanced chemoluminescence procedure from Amersham. Exposures chosen for quantitation were in the linear range. The level of either α-actinin or ABP-120 was determined by scanning densitometry of two to three different exposures, which were averaged and then divided by the total intensity of an identical whole cell lane stained with Coomassie blue to obtain the specific activity.

Triton-insoluble Cytoskeletons

Triton-insoluble cytoskeletons were prepared according to the method of Dharmawardhane *et al.* (1989). The actin content in the cytoskeletons was quantitated by scanning densitometry of the 42-kDa actin band on Coomassie blue-stained gels. The levels of ABP-120 in the cytoskeleton were determined by Western blotting and quantitation by scanning densitometry.

Confocal Microscopy

Immunofluorescence of Starved Cells. Cells were prepared for fluorescence microscopy according to the method of Cox *et al.* (1992). Cells were fixed 40–50 s after stimulation with 1 μM 2′ deoxy cAMP after 6 h of starvation. Cells were stained for the presence of

ABP-120 using an anti-ABP-120 polyclonal antibody with a fluorescein-labeled goat anti-rabbit secondary antibody (Cappel, Organon Teknika, Durham, NC), and stained for F-actin using rhodamine phalloidin.

Immunofluorescence of Cells During Phagocytosis. Mid-log phase cells, grown in HL5, were washed once in 20 mM $Na/K/PO_4$ buffer and resuspended to a final density of 2×10^6 cells/ml. Aliquots of 100 μl of cells were placed on ethanol cleaned glass coverslips and allowed to adhere for 30 min at 21°C. Rhodamine-labeled 1-μm latex beads (Fluorospheres, Molecular Probes) were added to the cells and allowed to settle for 20 min at 4°C. At this temperature the beads will bind to the cell surface but will not be internalized (Cohen *et al.*, 1994). The coverslips were warmed to 21°C to start phagocytosis and then fixed at various times (from 5–30 min). Cells were stained for the presence of ABP-120 using an anti-ABP-120 polyclonal antibody with a cy5-labeled goat anti-rabbit secondary antibody (Cappel, Organon Teknika) and stained for F-actin using fluorescein phalloidin.

Stained slides were examined on a Bio-Rad MRC-600 laser scanning confocal microscope using a Nikon 60× 1.4 numerical aperture planapochromat objective as described by Cox *et al.* (1995).

Electron Microscopy

Cells were prepared for electron microscopy according to the method of Cox *et al.* (1995) with minor modifications. Cells were starved for 6 h in 20 mM $Na/K/PO_4$ and then allowed to adhere to ethanol cleaned, glow discharged polylysine-coated coverslips for 5 min. Cells were permeabilized for 2 min in DICTY PHEM buffer (15 mM piperazine-*N*,*N*′-bis(ethansulfonic acid), 6.25 mM *N*-2-hydroxyethylpiperazine-*N*′-2-ethanesulfonic acid, 10 mM EGTA, 0.5 mM $MgCl_2$, pH 6.9) containing 0.75% Triton X-100, 5 μM phallacidin, and protease inhibitors directly or after stimulation with 1 μM 2′ deoxy cAMP for 40 s. Cytoskeletons were fixed in DICTY PHEM buffer containing 2% gluteraldehyde (Polysciences, Warrington, PA) for 15 min. The coverslips were extensively washed in glass-distilled water, rapidly frozen, freeze dried, and rotary coated with platinum without rotation in a Cressington CFE-50 freeze fracture apparatus (Cressington Scientific Instruments, Watford, UK). For the determination of pseudopod thickness, the Z-axis height of filaments in cytoskeletons was determined from paired stereo micrographs as described previously (Hartwig and Shevlin, 1986).

Computer-assisted Behavioral Analyses

General cell motility parameters were analyzed according to methods previously described (Soll, 1988; Soll *et al.*, 1988; Cox *et al.*, 1992) with points particularly relevant to this study summarized below. In brief, cells were grown to mid-log phase in HL5 medium at 22°C, washed free of nutrients, and dispersed on black Whatman No. 29 filters (Maidstone, UK) supported by prefilters and saturated with buffered salts solution (BSS; Soll, 1987). When cultures reached the ripple stage (the onset of aggregation), they were collected, washed free of nutrients, and used in motility analyses. Single cell behavior was analyzed in a Dvorak-Stotler chamber (Nicholson Precision Instruments, Gaithersburg, MD) perfused with BSS. Cells were videorecorded through differential interference contrast optics at 630× magnification and hand digitized into the data file of the DIAS program (Sylwester *et al.*, 1993; Soll, 1995). The parameters instantaneous velocity, directional change, length, area, and roundness were computed according to formulas previously described (Soll, 1988, 1995; Cox *et al.*, 1992). Positive flow was computed as the percentage area contained in the expansion zones of difference pictures, which were generated by overlapping images in frames separated by 4-s intervals (Soll, 1995).

In the analysis of pseudopod dynamics, a pseudopod was defined as an initially conical extension from the main cell body, which achieved a minimum area of 4 μm^2. Pseudopod area was measured from the base of the pseudopod, which was drawn as the continuation of the cell body contour. "Initial pseudopodial area" was defined as the % of total area that was in the pseudopod upon initial identification in observations made at 4-s intervals. "Average maximum rate of pseudopodial growth" was measured as the maximum % growth per 4-s interval during pseudopodial expansion. Comparison of videotaped segments of the digitized cells and digitized images demonstrated that in all cases, extensions analyzed as pseudopods represented extensions with anterior zones free of particulate cytoplasm and morphologies conforming to traditional pseudopods, and staining with fluorescein-phalloidin demonstrated that such extensions stained differentially for F-actin in their cortex during the expansion phase (Wessels *et al.*, 1989).

To analyze the behavioral effects of the rapid addition of 1 μM cAMP, the intake port of a Dvorak-Stodler chamber was connected to a T-valve. BSS was perfused for 5 min, and the valve then switched to BSS containing 1 μM cAMP. Dye analysis demonstrated that it took roughly 6 s for the cAMP solution to perfuse the chamber. Cells were continuously videorecorded before and after the addition of cAMP, and cell images digitized at 4-s intervals.

Analysis of Chemotactic Efficiency in a Spatial Gradient of cAMP. Cells were dispersed at low density on the bridge of a gradient chamber consisting of a plexiglass bridge bounded on either side by parallel troughs (Zigmond, 1977; Varnum-Finney *et al.*, 1987). One trough contained BSS, and served as a sink, and the other contained 1 μM cAMP, and served as a trough. Cells were allowed to acclimate for 4 min and then videorecorded for 12 min. The chemotactic index (C.I.) was computed from the centroid track as net distance moved toward the source divided by the total distance moved (McCutcheon, 1946). A C.I. of +1.0 represents a direct course toward the source and a C.I. of −1.0 represents a direct course away. A C.I. of 0.0 reflects complete randomness. Positive C.I.s between 0.0 and +1.0 reflect increasing levels of chemotactic efficiency (McCutchean, 1946).

RESULTS

Re-expression of ABP-120

The original ABP-120$^-$ cell lines were created by homologous recombination using a G418 resistance cassette for drug selection (Cox *et al.*, 1992). To re-express ABP-120 in the ABP-120$^-$ cell lines, a different selection procedure had to be employed. An ABP-120$^-$ cell line, AX3–1S-4$^-$ (Table 1), was transformed by electroporation with a linear disruption fragment of g7PYR5Δ 6.2, in which a fragment of the coding region of the PYR5–6 gene has been deleted. Ura$^-$ transformants were selected by their ability to grow in the presence of 5-fluoro-orotic acid. The resulting ABP-120$^-$/ura$^-$ cell line was then co-transformed with a vector containing a functional PYR5–6 gene and an ABP-120 expression vector. The ABP-120 expression vector contains the entire coding region of ABP-120, which is flanked 5′ and 3′ with an actin 15 promotor and an actin 8 terminator, respectively (Figure 1).

Transformants that were able to grow in the absence of uracil were then screened for the presence of ABP-120. In three separate transformations several independent ura$^+$ cell lines were isolated that re-expressed ABP-120 in various amounts. Two cell lines that expressed ABP-120 in wild-type amounts, one that was G418 resistant (3P-2), and one that was G418 sensitive

Table 1. Strains used in this study

Cell line	Phenotype	Description
AX3	ABP-120$^+$/ura$^+$/G418^S	Wild-type strain that was the parental cell line of the original ABP-120$^-$ and ABP-120$^+$ cell lines
1S-2	ABP-120$^+$/ura$^+$/G418^R	ABP-120$^+$ control transformed cell line (Cox *et al.*, 1992)
1S-4	ABP-120$^-$/ura$^+$/G418^R	Original ABP-120$^-$ cell line (Cox *et al.*, 1992) that was used for transformation in this study
3P-2	ABP-120$^{-/+}$/ura$^+$/G418^R	"Rescued" cell line produced by co-transformation containing original multi-copy insertion (see Figure 1B)
5-7	ABP-120$^{-/+}$/ura$^+$/G418^S	Rescued cell line produced by co-transformation with loss of the original multi-copy insertion
1P-2	ABP-120$^-$/ura$^+$/G418^R	ABP-120$^-$ cell line that has been through all transformations as rescued cell lines but without the ABP-120 reexpression vector

(5–7), were chosen for further phenotype analysis. All cell lines used in this study are described in Table 1, while the strategy for their production is shown in Figure 1B.

Southern blots were performed to analyze the integration of the ABP-120 expression vector. Genomic DNA was digested with *Nde*I and hybridized with a probe made from the entire ABP-120 coding region. This probe should hybridize to both the native gene locus and any site into which the vector has integrated. In wild-type cells, *Nde*I cuts once upstream of the gene, once near the 3′ end of the gene, and once after the coding region, giving rise to two fragments of 2.8 and 4 kb (Figure 2A, lane 1 and Figure 2B). The original disruption of the ABP-120 gene locus resulted from a multi-copy insertion of the disruption vector, which can been seen in Southern blots as the absence of the 2.8-kb band and the appearance of a high molecular weight band corresponding to the multi-copy repeat (Figure 2A, lane 3 and Figure 2B). A control cell line 1P-2, transformed in the same manner as the rescued cell lines, but without the ABP-120 expression vector, was still ABP-120$^-$ but could grow in the absence of uracil (Figure 1B). Southern blot analysis of this ABP-120$^-$ control cell line (1P-2) showed a pattern identical to the original ABP-120$^-$ cell line (Figure 2A, compare lanes 3 and 4). Southern blot analysis of the rescued cell line 3P-2 showed a pattern similar to the original disruptant with the integration of at least two copies of the ABP-120 expression vector (Figure 2A, lane 5) and analysis of the rescued cell line 5–7 showed the loss of the multi-copy insertion (Figure 2A, lane 2). Additional Southern blots performed on 5–7 confirmed the loss of the multi-copy insertion consistent with re-expression of ABP-120 and the loss of G418 resistance in this cell line. However, the wild-type ABP-120 gene locus was not restored in the case of 5–7 as indicated by the appearance of an additional *Eco*RI site in the 5′ end of the gene due to the integration of the re-expression vector (our unpublished results).

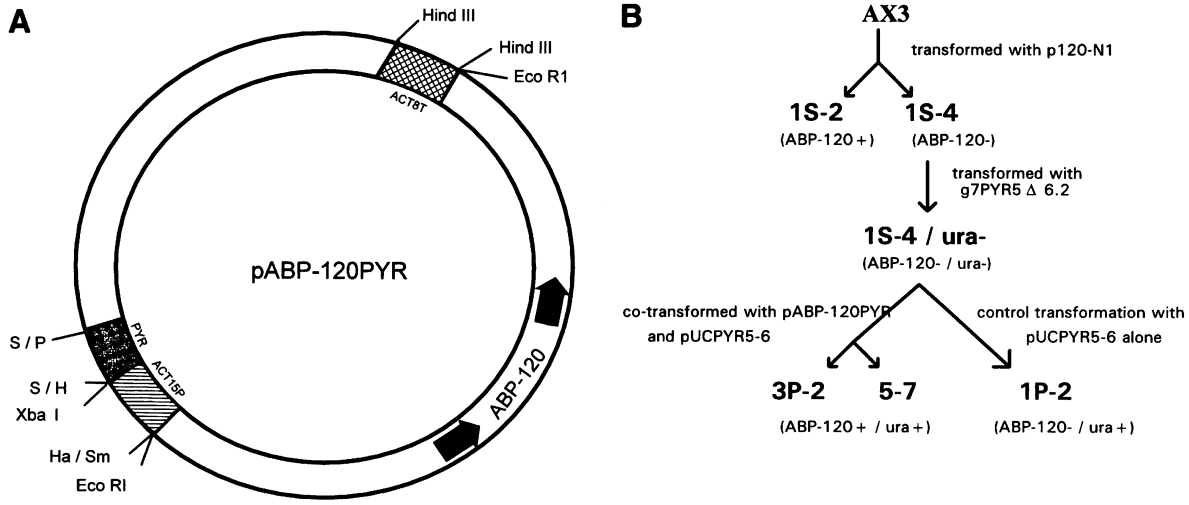

Figure 1. (A) The ABP-120 expression vector used to re-express ABP-120. The actin 15 promotor (cross hatched) was placed 5′ to the ABP-120 coding region, and the actin 8 terminator (boxed) was placed 3′ to the ABP-120 stop codon to create the ABP-120 expression cassette. A fragment of the pyr5–6 coding sequence (gray) was inserted. (B) Strategy for production of ABP-120$^{-/+}$ rescued cell lines.

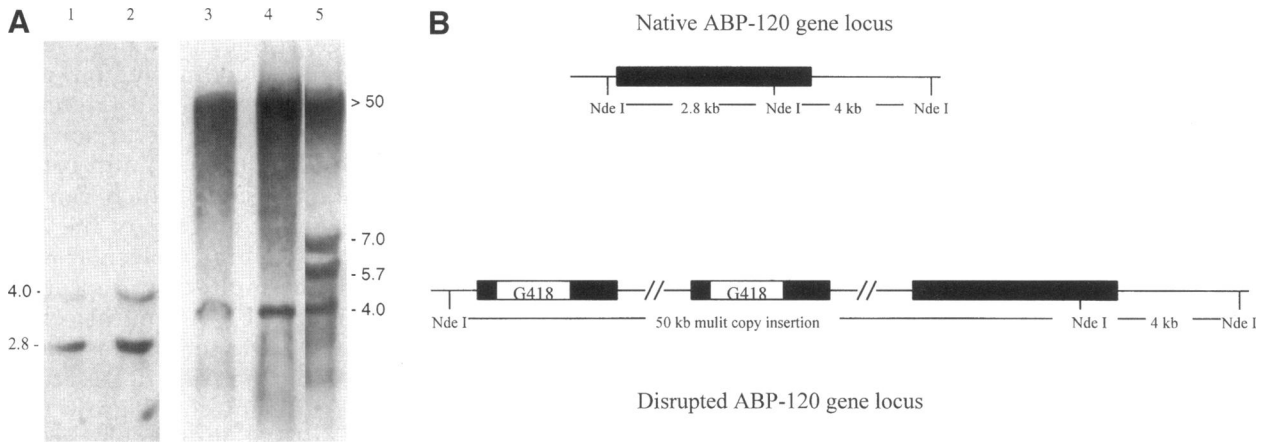

Figure 2. Southern blot analysis shows the integration of the ABP-120 expression cassette into the genome of ABP-120$^-$ cells. (A) Genomic DNA was digested with *Nde*I and probed with the coding region of ABP-120. Lane 1, AX3 (wild type); lane 2, ABP-120$^{-/+}$ (5–7) showing the loss of the multi-copy disruption; lane 3, parental ABP-120$^-$ cell line (1S-4$^-$) containing the multi-copy disruption; lane 4, ABP-120$^-$ transformation control (1P-2); and lane 5, ABP-120$^{-/+}$ (3P-2) containing the multi-copy insertion and the ABP-120 expression cassette. (B) Schematic diagram of the native ABP-120 gene locus and the disrupted ABP-120 gene locus in the original ABP-120$^-$ cell line.

Is There Compensation by Other Actin Binding Proteins?

In the past, when no phenotype was observed when a protein was deleted, it was postulated that there was compensation by another protein (Bray and Vasiliev, 1989; Gerisch *et al.*, 1989). In the present study it was necessary to demonstrate that re-introduction of ABP-120 expression and the constructs used in the integration and selection strategy did not affect the levels of synthesis of other major and/or related actin binding proteins that might suppress the ABP-120$^-$ phenotype, as proposed previously for α-actinin (Witke *et al.*, 1992).

In Table 2 the amounts of several different actin binding proteins found in vegetative or 6-h starved cells are shown. The two ABP-120$^{-/+}$ cell lines express wild-type amounts of ABP-120 while both the original ABP-120$^-$ cell line (1S-4) and the ABP-120$^-$ transformed control cell line (1P-2) do not express detectable amounts of ABP-120. The levels of the related actin binding proteins ABP-240, or *Dictyostelium* filamin, and α-actinin were analyzed, as was myosin II and actin for all of the cell lines. There was no detectable difference in any of the proteins analyzed in any of the cell lines studied.

Incorporation of Actin into the Cytoskeleton

Incorporation of actin into the cytoskeleton results from a combination of actin polymerization and filament cross-linking (Dharmawardhane *et al.*, 1989; Condeelis *et al.*, 1990). Actin is incorporated into the

Table 2. Expression level of various actin binding proteins

Line	ABP-120[a]	α-actinin[a]	actin[a]	myosin[a]	ABP-280[a]
Vegetative Cells					
ABP-120$^+$ (1S-2)	1.36 ± .13	1.22 ± .39	1.04 ± .07	1.28 ± .18	.75 ± .19
ABP-120$^-$ (1S-4)	0	1.58 ± .18	1.02 ± .06	1.28 ± .15	.91 ± .13
ABP-120$^-$ (1P-2)	0	1.44 ± .27	1.04 ± .13	1.16 ± .14	.97 ± .20
ABP-120$^{-/+}$ (5-7)	.98 ± .11	1.26 ± .31	1.03 ± .08	1.05 ± .10	.77 ± .19
ABP-120$^{-/+}$ (3P-2)	1.54 ± .18	1.67 ± .33	1.04 ± .06	1.43 ± .11	1.10 ± .17
After 6 h of starvation					
ABP-120$^+$ (1S-2)	.72 ± .07	1.09 ± .19	.82 ± .07	.96 ± .08	1.26 ± .13
ABP-120$^-$ (1S-4)	0	1.11 ± .17	.91 ± .09	.97 ± .11	1.03 ± .15
ABP-120$^-$ (1P-2)	0	1.01 ± .06	.85 ± .09	.95 ± .09	.86 ± .13
ABP-120$^{-/+}$ (5-7)	.86 ± .12	.96 ± .10	.86 ± .05	.88 ± .09	.90 ± .11
ABP-120$^{-/+}$ (3P-2)	1.20 ± .41	1.30 ± .54	1.03 ± .08	1.24 ± .10	1.35 ± .13

[a] Number equals the amount of the indicated protein/amount of total cell protein in mutant divided by the same in wild-type cells.

cytoskeleton in three peaks following cAMP stimulation, an initial peak at 5–10 s and second and third poorly resolved peaks between 30 and 60 s. It is during the second and third peaks of actin incorporation, which also correlate with pseudopod extension, that ABP-120 becomes incorporated into the cytoskeleton, suggesting that ABP-120 plays a role in the cross-linking of filaments into the cytoskeleton at these times (Dharmawardhane *et al.*, 1989; Cox *et al.*, 1992).

In the original ABP-120$^-$ cell lines it was shown that there was no alteration in the amount of actin polymerized in response to cAMP. However, unlike ABP-120$^+$ cells, ABP-120$^-$ cells do not incorporate actin into the Triton-insoluble cytoskeleton at 30–50 s (Cox *et al.*, 1992, 1995), indicating that the ABP-120$^-$ cells are defective not in the ability to polymerize actin but in the ability to incorporate actin into the cytoskeleton, consistent with the proposed role of ABP-120 in cross-linking actin filaments.

If ABP-120 is responsible for the cross-linking of actin filaments into the Triton-insoluble cytoskeleton, then re-expression of ABP-120 in an ABP-120$^-$ background should restore the incorporation of actin into the cytoskeleton between 30 and 60 s. The kinetics of incorporation of actin into the Triton-insoluble cytoskeleton was analyzed in the rescued cell lines and compared with an ABP-120$^+$ and ABP-120$^-$ control cell line (Figure 3). The ABP-120$^-$ control cell line 1P-2 showed a statistically significant reduction in the incorporation of F-actin into the cytoskeleton between 30 and 50 s, with a p value of ≤ 0.05, similar to that seen with the original ABP-120$^-$ cell line (Cox *et al.*, 1995). Both rescued cell lines, however, showed normal incorporation of actin into the Triton-insoluble cytoskeleton at times when the incorporation of actin is dramatically reduced in ABP-120$^-$ cells. The kinetics of incorporation of actin in ABP-120$^{-/+}$ cells is similar to that seen in ABP-120$^+$ cells, with p values of 0.327 and 0.221 for 3P-2 and of 0.706 and 0.515 for 5–7 at 30 and 50 s, respectively. However, in the 5–7 cell line there appeared to be a slight delay in the appearance of the second peak of actin incorporation (Figure 3). Consistent with the increase of actin incorporation into the cytoskeleton, both ABP-120 rescued cell lines showed levels of incorporation of ABP-120 into the cytoskeleton similar to that of wild-type cells (our unpublished observations).

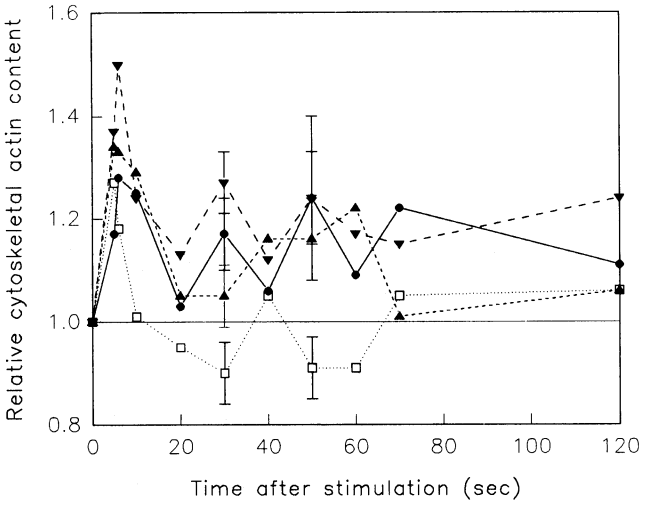

Figure 3. Re-expression of ABP-120 in ABP-120$^-$ cells restores the cross-linking of F-actin into the cytoskeleton 30–60 s following stimulation. Comparison of the kinetics of changes in relative actin content present in Triton-insoluble cytoskeletons following stimulation. (●) 1S-2 (ABP-120$^+$); (□) 1P-2 (ABP-120$^-$); (▼) 3P-2 (ABP-120$^{-/+}$); and (▲) 5–7 (ABP-120$^{-/+}$).

Immunofluorescence Analysis

Incorporation of ABP-120 into the cytoskeleton occurs at the same time as the appearance of cell surface projections, and ABP-120 has been localized to newly formed pseudopods after cAMP stimulation (Condeelis *et al.*, 1988; Hall *et al.*, 1988). Deletion of ABP-120 results in the reduction of the number of surface projections produced following stimulation when compared with ABP-120$^+$ control cells (Cox *et al.*, 1992, 1995). Immunofluorescence microscopy of typical stimulated ABP-120$^-$ cells showed that few surface projections were produced in response to cAMP (Figure 4, row 1) at a time when pseudopods were normally extended (Cox *et al.*, 1995). There was no staining of ABP-120 in ABP-120$^-$ cells (our unpublished observations), as was seen previously (Cox *et al.*, 1995). Immunofluorescence microscopy of typical stimulated rescued cells (Figure 4, rows 2 and 3) showed a greater number of surface projections compared with the ABP-120$^-$ cells. These surface projections contained the re-expressed ABP-120 and F-actin and are indistinguishable from wild-type projections (Cox *et al.*, 1995).

Electron Microscopy

Deletion of ABP-120 not only results in a decrease in the number of surface projections when compared with ABP-120$^+$ cells, but the surface projections that are produced by the ABP-120$^-$ cells are smaller in size (Cox *et al.*, 1992). For the electron microscope analysis, surface projections in contact with the substratum at the leading edge of a polarized cell were defined as pseudopods. When the pseudopods produced by ABP-120$^-$ cells were examined by transmission electron microscopy, they were found to be composed of a dense irregular network of actin filaments that is flatter than the regular filament networks of ABP-120$^+$ cells (Cox *et al.*, 1995). The filament networks in ABP-120$^-$ cells were aggregated into a mat in certain areas.

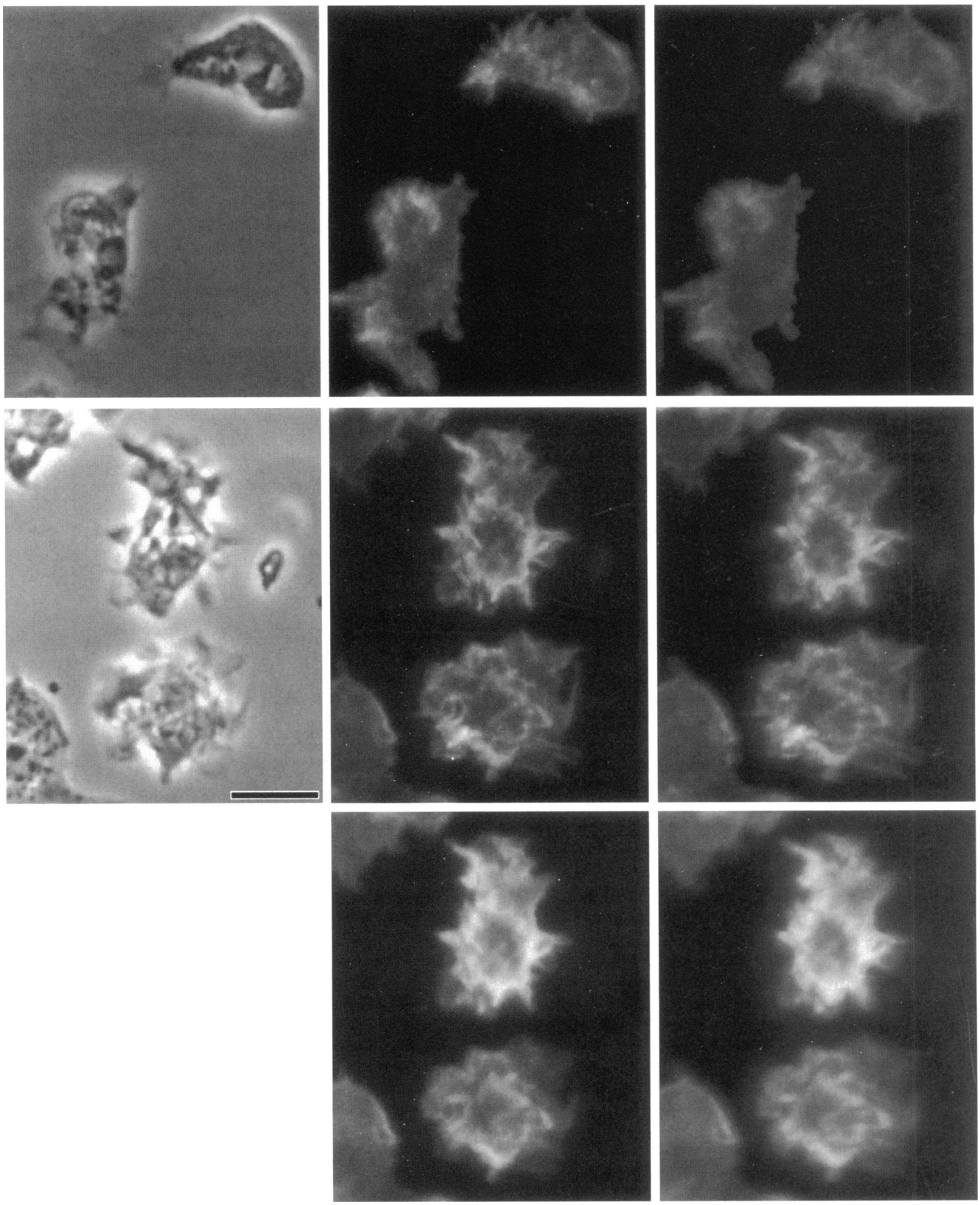

Figure 4.

The different organization of the actin filaments in ABP-120$^-$ pseudopods was consistent with the collapse of the filament network due to the absence of ABP-120–mediated cross-linking activity.

To determine whether the re-expression of ABP-120 in ABP-120$^-$ cells restores the normal filament network seen in pseudopods of ABP-120$^+$ cells, surface projections of the rescued cell lines were examined by transmission electron microscopy. Figure 5 shows a typical cytoskeleton from an ABP-120$^-$ cell (1P-2) and an ABP-120$^{-/+}$ cell (3P-2). As was seen previously (Cox *et al.*, 1995), pseudopods of ABP-120$^-$ cells were flatter in regions in which a majority of the filaments lie as a dense mat on the ventral surface of the cell with many foci of aggregated filaments. However, when cytoskeletons from ABP-120$^{-/+}$ rescued cells were analyzed, the pseudopods were found to be composed of a thicker three-dimensional network of long straight filaments (Figure 5 and Table 3), similar in appearance to those of ABP-120$^+$ cells (Cox *et al.*, 1995). Cytoskeletons of ABP-120$^{-/+}$ cells were differentiated from those of ABP-120$^-$ cells based on filament network morphology and pseudopod thickness, in a blind study, with an accuracy of greater than 80%. Therefore, not only do ABP-120$^{-/+}$ cells produce a larger number of pseudopods than ABP-120$^-$ cells, the pseudopods that they produce are wild-type in size, thickness, and filament network morphology.

Motion Analysis

Normalization of behavior in buffer. We previously demonstrated that ABP-120$^-$ cells translocate in buffer at a reduced average instantaneous velocity and exhibit an increase in mean directional change (i.e., a decrease in directionality) (Cox *et al.*, 1992). We, therefore, first tested whether cells of the rescued (ABP-120$^{-/+}$) strains 3P-2 and 5–7 had the general motility characteristics of an ABP-120$^+$ control cell line (1S-2). Both ABP-120$^{-/+}$ cell lines exhibited average instantaneous velocities comparable to that of the control cell line, while cells of the ABP-120$^-$ cell line 1P-2 translocated at a depressed average instantaneous velocity (Table 4A). The return of instantaneous velocity (a measure based on centroid position) in the ABP-120$^{-/+}$ cell lines from the low level of ABP-120$^-$ cells to that of the ABP-120$^+$ control cell line 1S-2 was accompanied by an increase in positive flow (the percent of total cell area in expansion zones per 4-s interval) to that of the ABP-120$^+$ control cell line (Table 4A). In addition, both ABP-120$^{-/+}$ cell lines exhibited a return of directional change, from the high level exhibited by ABP-120$^-$ cells to the low level exhibited by the ABP-120$^+$ cell line (Table 4A). Resumption of instantaneous velocity and positive flow to wild-type levels suggests that the rate of locomotion and, therefore, of pseudopod extension has returned to normal after the re-expression of ABP-120.

In Figure 6, centroid and perimeter tracks are presented for two representative control ABP-120$^+$ (1S-2) cells (Figure 6A), two representative ABP-120$^-$ (1P-2) cells (Figure 6B), two representative 3P-2 (ABP-120$^{-/+}$) cells (Figure 6C), and two representative 5–7 (ABP-120$^{-/+}$) cells (Figure 6D), all translocating in buffer. It is clear that while the 1P-2 tracks are more compacted due to a decrease in instantaneous velocity and are usually wider due to greater direction change, the tracks of the two rescued ABP-120$^{-/+}$ cell lines 3P-2 and 5–7 are extended and trimmer due to the increase in instantaneous velocity and decrease in directional change, respectively. In all respects, the tracks of cells of both rescued cell lines (Figure 6, C and D) are indistinguishable from those of the ABP-120$^+$ control cell line (Figure 6A).

We also demonstrated previously that ABP-120$^-$ cells translocating in buffer were, on average, shorter and rounder than control ABP-120$^+$ cells (Cox *et al.*, 1992), even though the average area, and presumably the volume, of control and mutant cells were similar (Cox *et al.*, 1992). The rescued cell lines exhibited length and roundess parameters similar to the ABP-120$^+$ control cell line (Table 4A). Again, area was similar between the ABP-120$^+$ cell line, the ABP-120$^-$ cell line 1P-2, and the two rescued cell lines 3P-2 and 5–7 (Table 4A). Together, these results demonstrate that the rescued cell lines have reestablished both the original behavioral and morphological phenotype of wild-type cells translocating in buffer.

We previously demonstrated that ABP-120$^-$ cells translocating in buffer formed fewer pseudopods per unit time and that the pseudopodial projections of ABP-120$^-$ cells, on average, achieved smaller maximum areas than control ABP-120$^+$ cells. The frequency and size of pseudopodial projections, identified and defined according to the rules presented in MATERIALS AND METHODS, were compared between control, mutant, and rescued cells (Table 5). The frequency of pseudopod formation by cells of the control ABP-120$^+$ cell line and the mutant ABP-120$^-$ cell line were 9.4 ± 3.8 and 4.9 ± 1.6 per 10 min, respectively. The frequency of pseudopod formation in the ABP-120$^{-/+}$ cell lines 3P-2 and 5–7 was not significantly different from the ABP-120$^+$ cell line, but

Figure 4 (cont). Immunofluorescence micrographs of typical stimulated ABP-120$^-$ cells compared with typical stimulated ABP-120$^{-/+}$ cells. (Row 1) Pseudo-phase image of 1S-4 cells (ABP-120$^-$) and corresponding stereo pair of the same cell with F-actin stained with rhodamine phalloidin. (Row 2) Pseudo-phase of 3P-2 cells (ABP-120$^{-/+}$) and corresponding stereo pair showing F-actin. (Row 3) Stereo pair of the same cells as in (row 2) stained for the presence of ABP-120. Cells were prepared and imaged under identical conditions. The cells in row 1 were in the same field of view in the microscope and have been moved closer together to appear in the same panel. Bar, 10 μm.

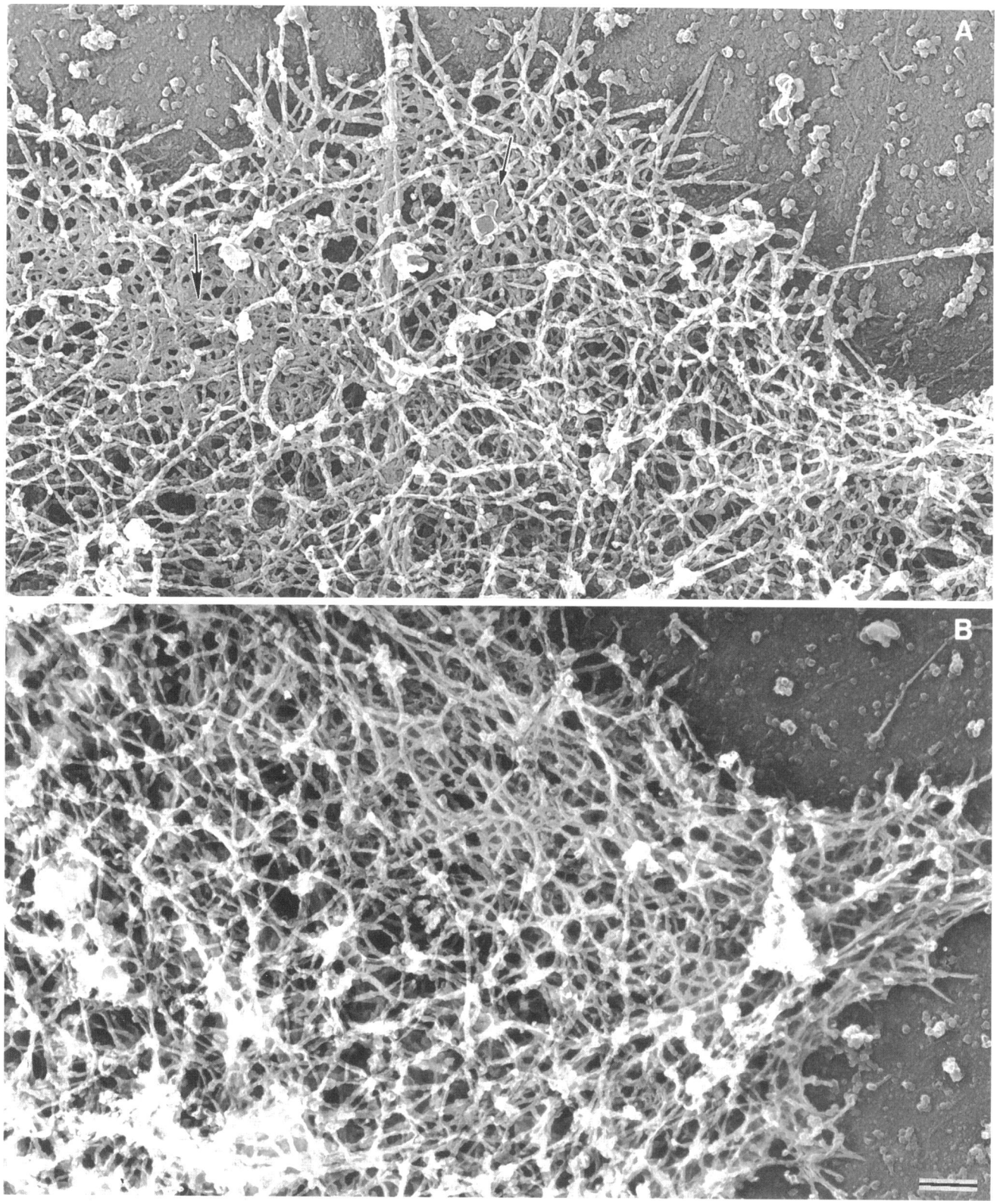

Figure 5.

significantly different from the ABP-120$^-$ cell line (Table 5). In addition, the mean maximum rate of pseudopodial growth of the ABP-120$^+$ control cell line and of the ABP-120$^{-/+}$ cell lines was not significantly different, but significantly different from the mutant ABP-120$^-$ cell line (Table 5). Therefore, the decrease in the frequency and maximum rate of pseudopod expansion by ABP-120$^-$ cells was normalized in both rescued cell lines.

Normalization of behavior after the rapid addition of cAMP. We previously demonstrated that within seconds after ABP-120$^-$ cells were treated with the rapid addition of 1 μM cAMP, they underwent a decrease in instantaneous velocity that was modest in comparison to the decrease displayed by ABP-120$^+$ cells, primarily because the cells were already moving at a reduced velocity (Cox *et al.*, 1992). More importantly, ABP-120$^-$ cells did not exhibit the cyclic rebound in instantaneous velocity correlated with pseudopod extension exhibited by the ABP-120$^+$ control cells (Cox *et al.*, 1992). We therefore tested whether ABP-120$^{-/+}$ cells reacquired the behavioral response to the rapid addition of 1 μM cAMP exhibited by ABP-120$^+$ control cells. Cells of the ABP-120$^+$ control cell line (1S-2), the ABP-120$^-$ cell line (1P-2), and the two ABP-120$^{-/+}$ cell lines (3P-2 and 5–7) were individually inoculated into Dvorak-Stotler chambers and allowed to adhere to and resume translocation on the glass wall. Cells were then perfused first with buffer for 5 min, and then with a solution containing 1 μM cAMP for 10 additional minutes. Figure 7 shows the average instantaneous velocity of ABP-120$^+$ control cells, ABP-120$^-$ cells, and ABP-120$^{-/+}$ cells (3P-2 and 5–7). The estimated cAMP concentration in the perfusion chamber is diagrammed at the top as a function of time, and the mean instantaneous velocity is plotted during the 1.5 min preceding and the 3.5 min following addition of cAMP. As previously reported (Cox *et al.*, 1992), the mean instantaneous velocity of ABP-120$^+$ cells, which averaged 16 μm per min before cAMP addition, decreased to a low value of less than 4 μm per min within 20 s after cAMP first entered the chamber. Instantaneous velocity then exhibited a partial, cyclic rebound pattern (Figure 7). The instantaneous velocity of ABP-120$^-$ cells that averaged 4.3 μm per min before addition, decreased to an average value of 2.3 μm per min after addition, and showed no cyclic rebound after addition (Figure 7). Both the rescued cell lines 3P-2 and 5–7 underwent a decrease from an average instantaneous velocity of 16 μm per min to less than 4 μm per min within 20 s after cAMP first entered the chamber, and then exhibited a pattern of cyclic rebound. A delay in the rebound response is seen in the 5–7 cell line when compared with the ABP-120$^+$ control cell line and the rescued cell line 3P-2. This delay in rebound is consistent with the delay in the amount of actin incorporation into the cytoskeleton following cAMP stimulation seen in the 5–7 cell line (Figure 3). Otherwise, both rescued cell lines reestablished every aspect of the normal response to the rapid addition of 1 μM cAMP.

Table 3. Cytoskeletal thickness in ABP-120$^-$ and ABP-120$^{-/+}$ pseudopods

Distance from cytoskeletal margin	ABP120$^-$ (1P-2) cytoskeletal height (μm) ± SD (n = 10)	ABP-120$^{-/+}$ (3P-2) cytoskeletal height (μmm) ± SD (n = 10)
Edge	0.22 ± 0.10	0.41 ± 0.28
1 μm	0.31 ± 0.12	0.69 ± 0.29
2 μm	0.49 ± 0.29	1.00 ± 0.40

Normalization of efficient chemotaxis in a spatial gradient of cAMP. We previously demonstrated that ABP-120$^-$ cells exhibited a dramatic decrease in the efficiency of chemotaxis in a spatial gradient of cAMP. We, therefore, tested whether the ABP-120$^{-/+}$ cell lines reacquired the wild-type level of chemotactic efficiency by comparing motility and morphological parameters, as well as the chemotactic index, of the ABP-120$^+$ cell line, the ABP-120$^-$ cell line, and the two ABP-120$^{-/+}$ cell lines in a spatial gradient of cAMP generated in a gradient chamber (Zigmond, 1977; Varnum and Soll, 1984: Varnum-Finney *et al.*, 1987). As was observed in buffer (Table 4A), ABP-120$^-$ cells exhibited depressed mean instantaneous velocity, depressed mean positive flow, a decrease in length, and an increase in roundness when compared with ABP-120$^+$ cells (Table 4B). Interestingly, ABP-120$^-$ cells exhibited approximately the same mean directional change as wild-type cells in a spatial gradient (Table 4B), which may reflect the inhibition of lateral pseudopod formation observed when cells are placed in a spatial gradient of cAMP (Varnum-Finney *et al.*, 1987). More importantly, all of the behavioral and morphological defects were normalized in the two rescued cell lines (Table 4B).

To compare the efficiency of chemotaxis, we also computed the chemotactic index of individual cells based upon the direction of the source of attractant as described in MATERIALS AND METHODS. Cells of the ABP-120$^+$ control cell line exhibited a mean chemotactic index of +0.39 and cells of the ABP-120$^-$ cell

Figure 5 (cont). Comparison of the actin filament organization in pseudopods from ABP-120$^-$ cells and ABP-120$^{-/+}$ cells. (A) Structure of actin filaments in a representative pseudopod from a stimulated ABP-120$^-$ cell (1P-2). Arrows indicate regions of aggregated filaments. (B) Structure of actin filaments in a representative pseudopod from an ABP-120$^{-/+}$ rescued cell (3P-2). The actin filaments within this pseudopod have the appearance of those inside projections from wild-type cells, i.e., filaments are straight and organized into space-filling orthogonal networks.

Table 4A. Motility parameters of ABP-120$^+$ (1S-2), ABP-120$^-$ (1P-2), and ABP-120$^{\pm}$ cell lines (3P-2 and 5-7) translocating in buffer

Cell line	N	Inst. vel.[a] (μm/min)	Pos. flow[a] (%/4 s)	Dir. change[a] (deg.)	Length[a] (μm)	Area[a] (μm^2)	Roundness[a] (%)
ABP-120$^+$ (1S-2)	13	12.4 ± 3.6	12.0 ± 6.9	25.9 ± 6.9	21.8 ± 3.6	88.3 ± 15.3	39.4 ± 6.9
ABP-120$^-$ (1P-2)	44	6.0 ± 2.4	8.8 ± 3.0	42.9 ± 14.4	16.2 ± 3.4	85.0 ± 17.3	57.0 ± 10.8
ABP-102$^{-/+}$ (3P-2)	43	13.7 ± 3.6	12.1 ± 3.9	25.9 ± 6.9	20.1 ± 4.6	88.4 ± 18.6	40.1 ± 10.3
ABP-102$^{-/+}$ (5-7)	40	11.6 ± 3.2	14.6 ± 4.4	29.9 ± 6.9	19.3 ± 3.0	87.4 ± 18.2	46.0 ± 6.1
p values[b]							
1S-2 vs. 1P-2		<0.0001	<0.0005	<0.0001	<0.0005	NS	<0.0001
3P-2 vs. 1P-2		<0.0001	<0.0001	<0.0001	<0.0005	NS	<0.0001
5-7 vs. 1P-2		<0.0001	<0.0001	<0.0001	<0.0005	NS	<0.0001

Table 4B. In a spatial gradient of cAMP

Cell line	N	Inst. vel.[a] (μm/min)	Pos. flow[a] (%/4 s)	Dir. change[a] (deg.)	Length[a] (μm)	Area[a] (μm^2)	Roundness[a] (%)	Chemotactic index[a]
ABP-120$^+$ (1S-2)	15	13.5 ± 3.9	9.9 ± 6.9	20.2 ± 14.3	19.6 ± 3.1	79.1 ± 19.0	39.4 ± 6.9	0.39
ABP-120$^-$ (1P-2)	25	5.0 ± 2.7	5.4± 2.2	22.1 ± 17.1	14.7 ± 2.1	68.5 ± 13.9	57.0 ± 10.8	0.13
ABP-102$^{-/+}$ (3P-2)	25	13.1 ± 4.0	10.0 ± 3.9	18.9 ± 10.0	20.5 ± 3.4	78.6 ± 15.4	40.1 ± 10.3	0.38
ABP-102$^{-/+}$ (5-7)	26	12.9 ± 4.8	9.5 ± 3.1	19.5 ± 11.9	19.4 ± 3.8	76.2 ± 18.3	46.0 ± 6.1	0.42
p values[b]								
1S-2 vs. 1P-2		<0.0001	<0.0001	NS	<0.0001	NS	<0.0001	<0.0001
3P-2 vs. 1P-2		<0.0001	<0.0001	NS	<0.05	NS	<0.0001	<0.0001
5-7 vs. 1P-2		<0.0001	<0.0001	NS	<0.05	NS	<0.0001	<0.0001

[a] Values for instantaneous velocity (Inst. vel.), positive flow (Pos. flow), directional change (Dir. change), length, area, and roundness represent the means of N cells, each averaged over a period of 3 min or greater. The computations of these parameters are presented in MATERIALS AND METHODS.

[b] For all parameters, the *p* values for 1S-2 vs. 3P-2 and 1S-2 vs. 5-7 were not significant.

line exhibited a mean chemotactic index of +0.13 (Table 4B). The two rescued cell lines 3P-2 and 5–7 exhibited mean chemotactic indices of +0.38 and +0.42, which were statistically indistinguishable from the control ABP-120$^+$ cell line (Table 4B). These results demonstrate that both rescued cell lines reacquire the chemotactic efficiency of the wild-type strain.

Localization of ABP-120 to Phagocytic Cups

ABP-120 has been shown to be important in the formation of pseudopods produced in cells moving randomly in buffer and in response to the chemoattractant cAMP (Cox *et al.*, 1992). To determine whether ABP-120 is also involved in the formation of pseudopods produced during phagocytosis, an immunofluorescence analysis of *Dictyostelium* cells phagocytosing fluorescently labeled latex beads was performed. In Figure 8 a typical ABP-120$^+$ cell (1S-2) in the process of phagocytosing a latex bead is shown. The cell has produced an actin-filled pseudopod around the bead and ABP-120 is co-localized with the actin in this projection. If cells that no longer express ABP-120 (1P-2) are examined in the process of phagocytosis, it is seen that phagocytic cups that contain F-actin are not usually produced (Figure 8). However, when ABP-120 is re-expressed in the ABP-120$^-$ cells, normal phagocytic cups are seen (Figure 8).

This evidence not only shows that ABP-120 is found in phagocytic cups but also that ABP-120 may be important in the formation of the phagocytic cups. If this is true then the deletion of ABP-120 should have an effect on the ability of the cells to ingest particles.

ABP-120$^-$ Cells Show a Reduced Ability to Phagocytize Particles

The ability of both ABP-120$^+$ and ABP-120$^-$ cells to ingest particles in suspension was analyzed using a quantitative assay (Vogel *et al.*, 1980; Cohen *et al.*, 1994), the results of which are shown in Figure 9. The various cell lines were incubated with fluorescently labeled bacteria for 30 min and then the number of bacteria ingested was determined by comparison with a standard curve of known bacterial concentrations. ABP-120$^+$ cells (1S-2) ingested 74 ± 7 (± SEM) bacteria after 30 min. This value is similar to previously reported values for wild-type *Dictyostelium* cell lines (Vogel *et al.*, 1980; Cohen *et al.*, 1994). However, ABP-120$^-$ cells (1P-2) ingested only 28 ± 4 (± SEM) bacteria on average after 30 min. The difference in the number of bacteria ingested by ABP-120$^+$ and ABP-120$^-$ cells

is statistically significant, with a p value of 0.005 in a Student's *t* test. This twofold reduction can be restored to wild-type levels by the re-expression of ABP-120, with values of 60 ± 13 and 90 ± 8 (± SEM) bacteria ingested after 30 min and p values of 0.310 and 0.171 for 3P-2 and 5–7, respectively.

Mutant *Dictyostelium* cell lines have been isolated that have shown defects in phagocytosis when in suspension but regain the ability to phagocytize particles while attached to a substrate (Vogel *et al.*, 1980; Cohen *et al.*, 1994). Therefore, the ability of ABP-120$^+$ and ABP-120$^-$ cells to ingest particles while attached to a surface was also analyzed. Cells were allowed to attach to a glass coverslip and then fluorescently labeled latex beads were added at 4°C to allow the beads to bind but not be internalized. The cells were washed to remove unbound beads and then warmed to 21°C for 15 min to allow phagocytosis to take place. Phagocytosis was halted by fixation with gluteraldehyde and the cells were processed for confocal microscopy. By staining the cells for F-actin, which allows identification of the cell cortex, it is possible to use confocal microscopy to distinguish beads present on the outside versus inside of a cell. When 10 ABP-120$^+$ and 10 ABP-120$^-$ cells were analyzed in this manner, a similar twofold reduction in the number of particles ingested by ABP-120$^-$ cells was seen when compared with ABP-120$^+$ cells, 0.6 ± 0.2 (± SEM) beads per ABP-120$^-$ cell compared with 1.2 ± 0.3 (± SEM) beads per ABP-120$^+$ cell.

One of the possible explanations for a decrease in the rate of uptake of particles in phagocytic mutants is a defect in particle binding. This was seen to be the case in several previously isolated phagocytosis mutants (Vogel *et al.*, 1980). When 10 ABP-120$^+$ and 10 ABP-120$^-$ cells were analyzed by confocal microscopy, as described above, the same number of particles were found bound to the cell surface, 1.6 ± 0.4 (± SEM) beads per ABP-120$^-$ cell compared with 1.5 ± 0.4 (± SEM) beads per ABP-120$^+$ cell. Therefore, the decrease in the number of particles ingested by ABP-120$^-$ cells is not due to a defect in the binding of particles to the surface of the cell.

ABP-120$^-$ Cells Exhibit Growth Defects in Bacterial Suspensions

When *Dictyostelium* cells are grown in the presence of bacteria alone, survival is dependent on the ability of cells to perform phagocytosis. A decrease in the ability

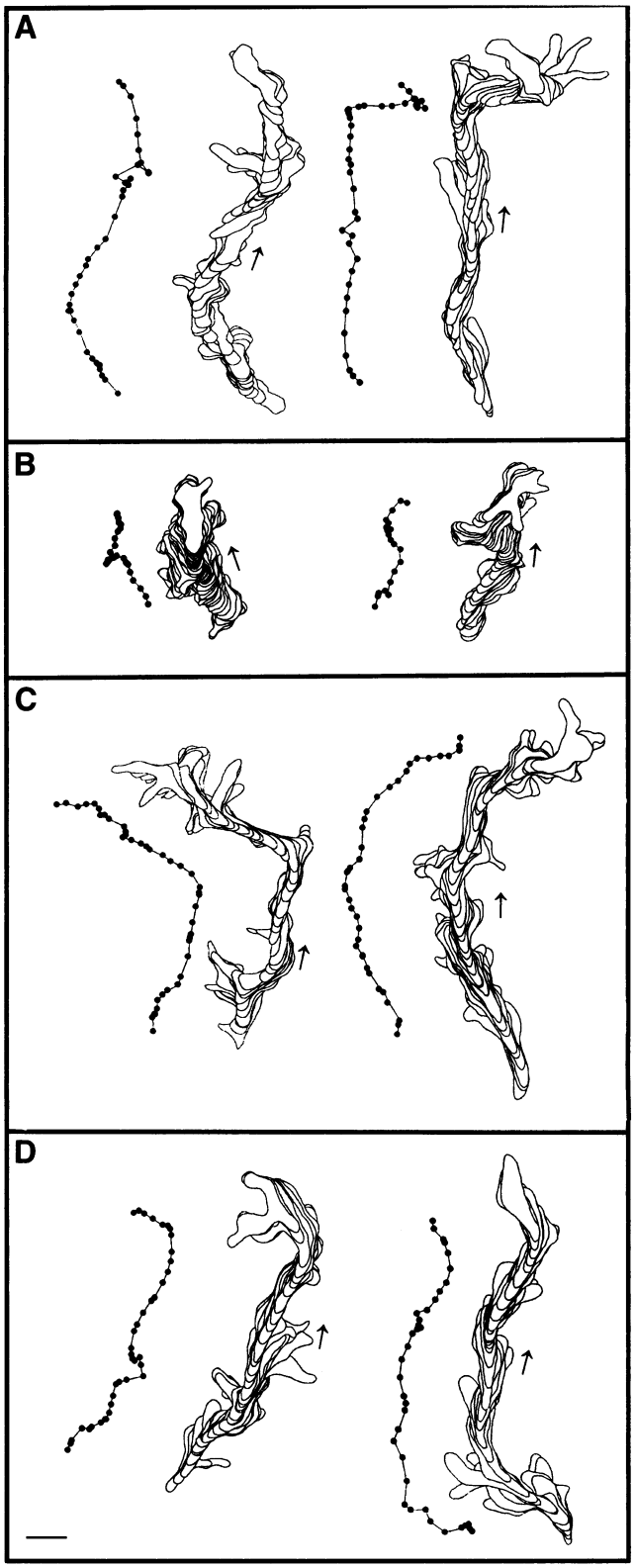

Figure 6. Centroid and cell perimeter plots of two representative cells of the control ABP-120$^+$ cell line 1S-2 (A), the mutant ABP-120$^-$ cell line 1P-2 (B), the rescued ABP-120$^{-/+}$ cell line 3P-2 (C), and the rescued ABP-120$^{-/+}$ cell line 5–7 (D). For the centroid and perimeter tracks in panels A, C, and D, the time interval was 8 s. For the centroid and perimeter tracks in panel B, the interval was 12 and 8 s, respectively. The arrows represent direction of translocation. The scale bar, in panel D, represents 10 μm.

Table 5. Dynamics of pseudopod extension of control ABP-120$^+$ (1S-2), ABP-120$^-$ (1S-4), and rescued ABP-120$^{-/+}$ (3P-2 and 5-7) cells translocating in buffer

Cell line	N	Number of pseudopods	Average number of pseudopods per 10 min[a]	Average initial pseudopodial area (%)[a]	Average maximum rate of pseudopodial growth (%/4 s)[a]
ABP-120$^+$ (1S-2)	11	84	9.4 ± 3.8	8.9 ± 4.1	19.5 ± 8.1
ABP-120$^-$ (1P-2)	20	98	4.9 ± 1.6	4.9 ± 4.0	7.4 ± 3.0
ABP-102$^{-/+}$ (3P-2)	20	193	9.7 ± 3.3	11.1 ± 5.2	18.9 ± 9.1
ABP-102$^{-/+}$ (5-7)	20	156	7.8 ± 2.9	9.7 ± 3.5	15.6 ± 6.9
p-value[b]					
1S-2 vs. 1P-2			<0.0001	<0.0001	<0.0001
3P-2 vs. 1P-2			<0.0001	<0.0001	<0.0001
5-7 vs. 1P-2			<0.0001	<0.0001	<0.0001

[a] The definition of pseudopods and the measured parameters are provided in MATERIALS AND METHODS.
[b] The *p* values between 1S-2 vs. 3P-2 and 1S-2 vs. 5-7 for all parameters were not significant.

of a cell to uptake particles should have an effect on the ability of a cell to grow in the presence of bacteria alone as a food source. To test this possibility, ABP-120$^+$ and ABP-120$^-$ cells were inoculated into bacterial suspensions and growth was monitored over time. The results of a typical experiment are shown in Figure 9. The ABP-120$^+$ cell line (1S-2) grew rapidly after an initial lag of 10 to 20 h, reaching a maximum density of 1.7×10^7 cells/ml after 30 h of incubation (Figure 9A). When the rate of bacterial clearance from the same suspension was monitored, it was observed that bacteria were removed from the culture when *Dicyostelium* multiplication became logarythmic (Figure 9B). The doubling time of ABP-120$^+$ cells in bacterial suspension, during log-phase growth, is approximately 3 h.

When two different ABP-120$^-$ cell lines (1S-4 and 1P-4) were analyzed, they both showed a decreased rate of growth in bacterial suspension and they both peaked at far lower cell densities than ABP-120$^+$ cells (Figure 9A). The rate of bacterial clearance in ABP-120$^-$ cultures was also reduced when compared with ABP-120$^+$ cultures (Figure 9B). The average doubling time of both ABP-120$^-$ cell lines was greater than 6 h during log phase and final cell density after 30 h was 2.5×10^6 cells/ml compared with 1.7×10^7 cells/ml for ABP-120$^+$ cells, almost a 10-fold reduction. Re-expression of ABP-120 normalized growth in bacterial suspension (Figure 9A). These results demonstrate that deletion of ABP-120 leads to cells that phagocytose bacteria at greatly reduced rates.

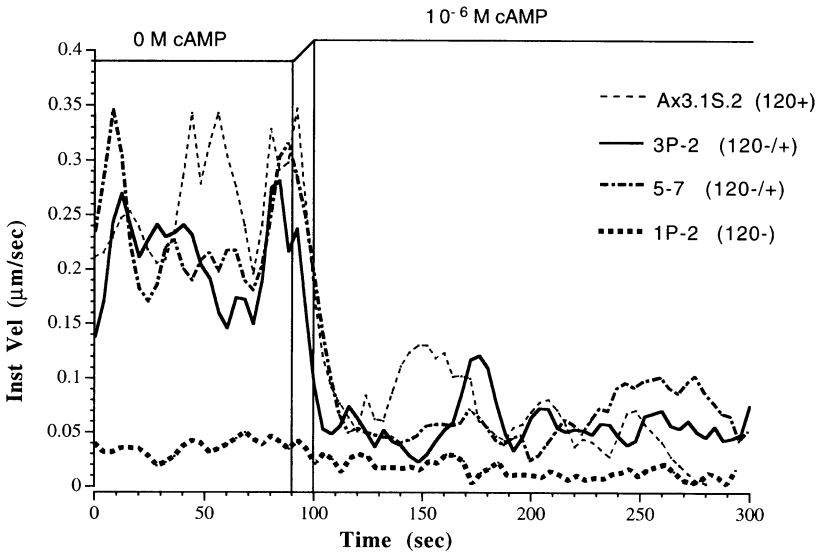

Figure 7. Instantaneous velocity before and after the rapid addition of 1 μM cAMP to cells of ABP-120$^+$ (AX3.1S.2), ABP-120$^-$ (1P-2), ABP-120$^{-/+}$ (3P-2), and the ABP-120$^{-/+}$ (5–7). In each case, data points used to generate the plots represent the average of five independently analyzed cells. At the top of the graph, the estimated concentration of cAMP in the chamber is diagrammed. Two vertical lines indicate the time at which cAMP first entered the chamber and the time the concentration reached 1 μM, respectively.

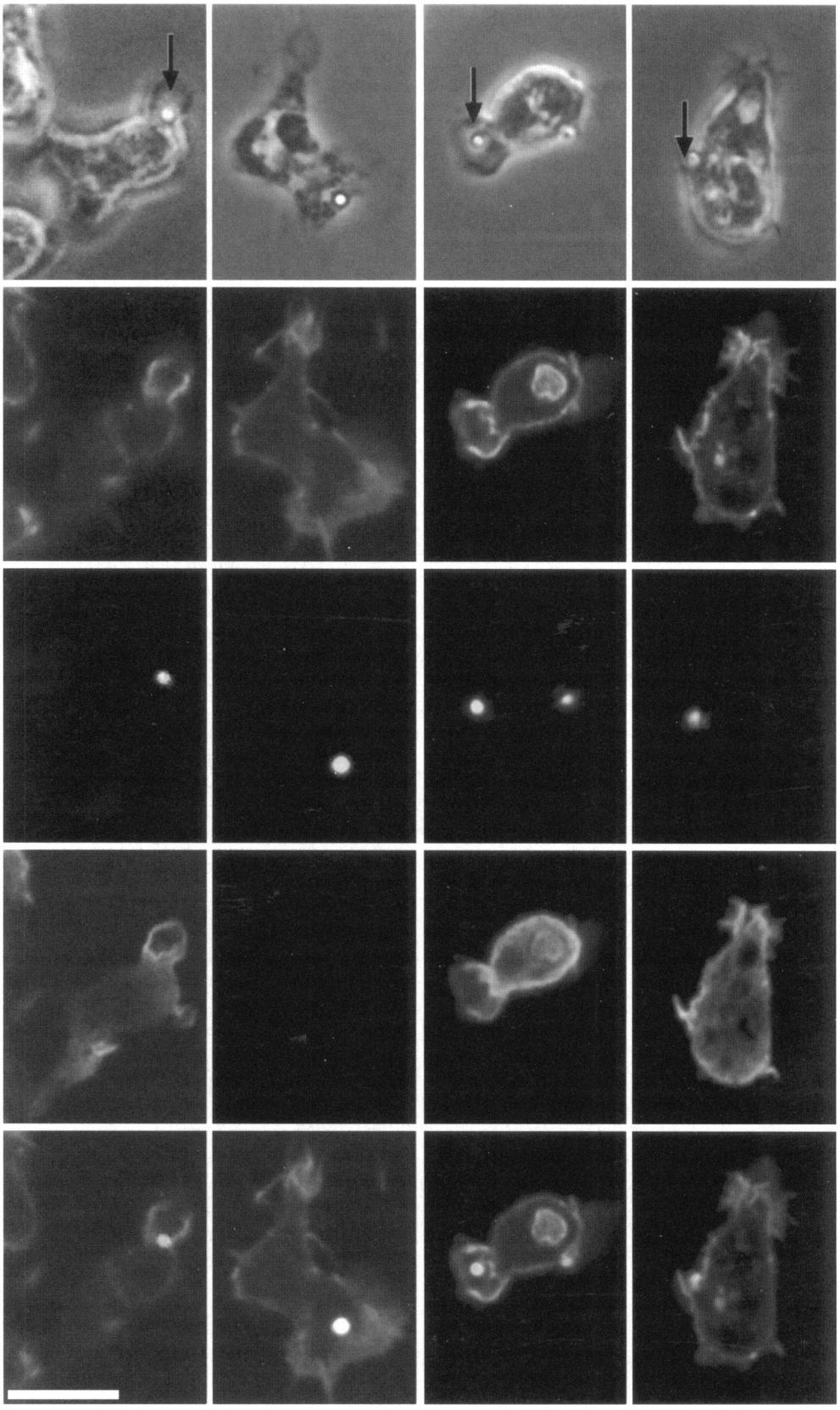

Figure 8. Immunofluorescence micrographs of cells engulfing latex beads, showing co-localization of F-actin and ABP-120 in phagocytic cups in ABP-120$^+$ cells (column 1) as compared with ABP-120$^-$ cells (column 2). Two different ABP-120$^{-/+}$ rescued cell lines are shown in columns 3 and 4 (3P-2 and 5–7, respectively). Each image represents a single optical section. A pseudophase image is shown for each cell (row 1). Images of the same cells shown in row 1 are shown in row 2 stained for the presence of F-actin with fluorescein phalloidin, in row 3 stained for the presence of the rhodamine bead, and in row 4 stained for the presence of ABP-120. There is no staining for ABP-120 in the ABP-120$^-$ cell, as shown previously (Cox *et al.*, 1992). (Row 5) A merged image of the actin and bead channel. Arrows indicate phagocytic cups. Scale bar, 10 μm.

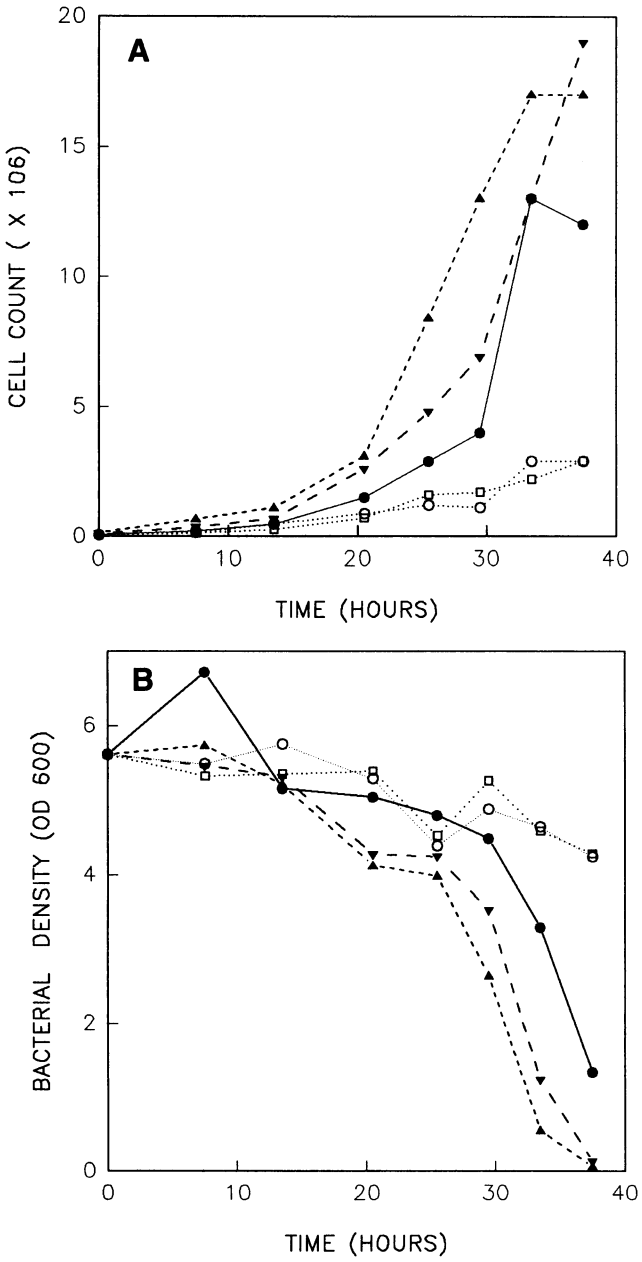

Figure 9. ABP-120$^-$ cells are defective in phagocytosis of and growth on bacteria in suspension. (A) The number of *Dictyostelium* cells in a bacterial suspension was measured over time. (B) For the same experiment the rate of bacterial clearance of the suspension was monitored by the decrease in density (OD 600). (●) 1S-2 (ABP-120$^+$), (○) 1S-4 (ABP-120$^-$), (□) 1P-2 (ABP-120$^-$), (▼) 3P-2 (ABP-120$^{-/+}$), and (▲) 5–7 (ABP-120$^{-/+}$).

Dictyostelium cells can obtain sustenance either by phagocytosis or pinocytosis. All of the cell lines used in this study were derived from an AX3 parental strain that is axenic and can grow in liquid culture by the process of pinocytosis. To determine if pinocytosis is affected by the deletion of ABP-120, ABP-120$^+$ (1S-2) and ABP-120$^-$ cell lines (1P-2 and 1S-4) were grown in liquid culture. ABP-120$^-$ cells grew with the same kinetics as ABP-120$^+$ cells, with a doubling time in liquid medium of approximately 10 h during log phase. Also, when ABP-120$^+$ and ABP-120$^-$ cells were allowed to pinocytose fluorescently labeled dextran there was no difference in the relative amount of dextran uptake between the two cell lines (our unpublished observations).

It was concluded that the defect in phagocytosis of ABP-120$^-$ cells had an effect on the ability of cells to grow when bacteria were provided as the sole source of nutrition, presumably by pseudopod-mediated phagocytosis, but there was no effect on the ability of mutant cells to grow in liquid medium by pinocytosis.

ABP-120$^-$ Cells Show Altered Colony Morphology When Grown on Bacterial Lawns

When a single *Dictyostelium* cell is placed on a lawn of bacteria, it ingests the bacteria by phagocytosis, multiplies, and eventually gives rise to a visible colony that appears as a small clearing in the bacterial lawn. As amoebae deplete the bacteria in the expanding colony, they begin to starve; starvation, in turn, initiates the developmental program. As development proceeds, individual cells stream into mounds that eventually differentiate into fruiting bodies. The presence of these various developmental stages within the colony imparts a characteristic morphology to it. That is, the different stages of development within the colony roughly form concentric rings. The outer edge of the colony containing feeding amoebae is followed centripetally by a zone of starving pre-aggregative cells, a zone of aggregating cells, a zone of intermediate morphologies, and fruiting bodies at the core, where the colony originated from a single cell (Soll, 1987). In some colonies, sectors with slightly altered morphology appear due to switching (Kraft, *et al.*, 1988).

We examined colony growth of both ABP-120$^+$ and ABP-120$^-$ cell lines on bacterial lawns (Figure 10), monitoring both the rate of expansion over time as well as the width of the clear zone (Figure 11). Colonies of ABP-120$^+$ cells (1S-2) expanded at a steady rate until the bacterial lawn was consumed. Distinct zones could be seen, with a clear zone at the edge of the colony and the various stages of development culminating in fruiting bodies in the center of the colony. When colonies of ABP-120$^-$ cells (1S-4) were compared under the same conditions, and after the same period of time (4 and 7 days) as colonies of ABP-120$^+$ cells, it could be seen that the ABP-120$^-$ colonies were smaller in size and the clear zone was proportionately reduced (Figure 11). However, ABP-120$^-$ cells still underwent normal development, which culminated in the formation of fruiting bodies in the colony center

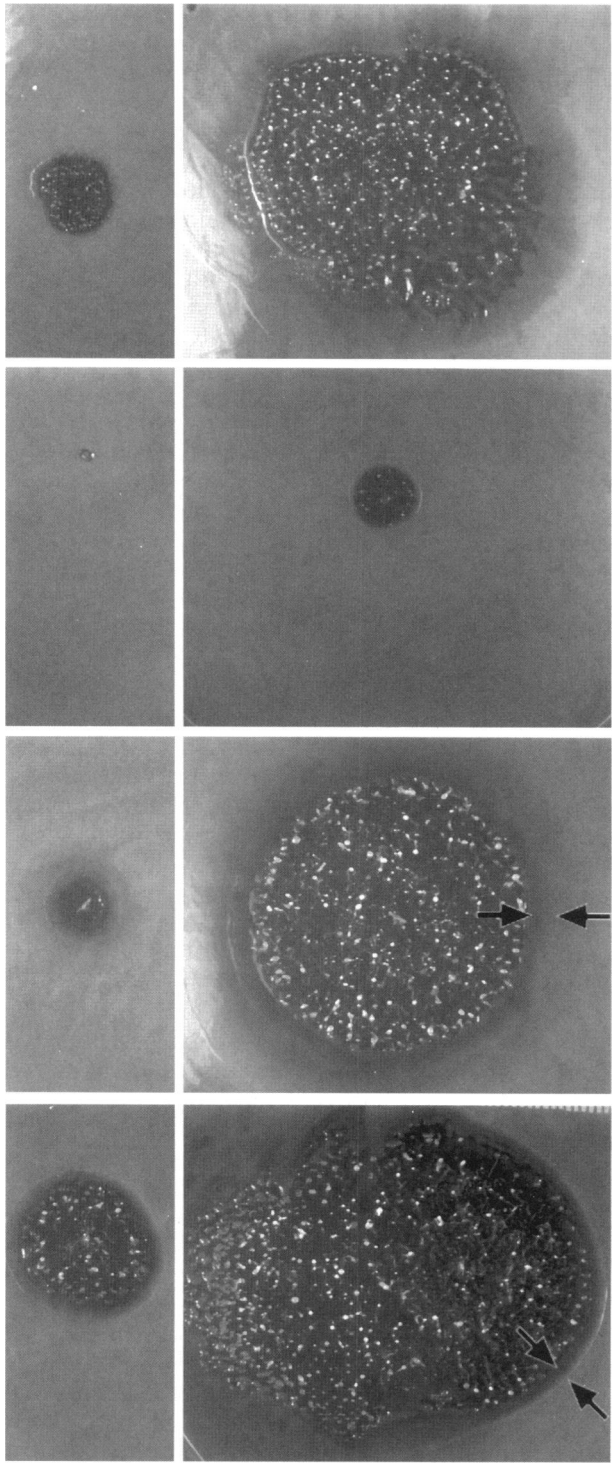

Figure 10. ABP-120$^-$ cells show an altered colony morphology when grown on bacterial lawns. Column 1, colonies after 4 days of growth; and column 2, after 7 days growth on KA lawns. (row 1) 1S-2 (ABP-120$^+$), (row 2) 1S-4 (ABP-120$^-$), (row 3) 3P-2 (ABP-120$^{-/+}$), and (row 4) 5–7 (ABP-120$^{-/+}$). All photographs are at the same magnification. The clear zone, or the zone in which the cells are active in phagocytosis, is indicated by the arrows. The colony in the upper left panel is approximately 1 cm in diameter.

(Figure 10). The difference in colony morphology between ABP-120$^+$ and ABP-120$^-$ cells was seen whether the colonies originated from single spores, single vegetative cells from HL5, or drops of vegetative cells from HL5 (our unpublished observations).

Re-expression of ABP-120 in ABP-120$^-$ cells, using an actin 15 promoter instead of the wild-type promoter, increased the rate of colony expansion and clear zone width when compared with colonies of

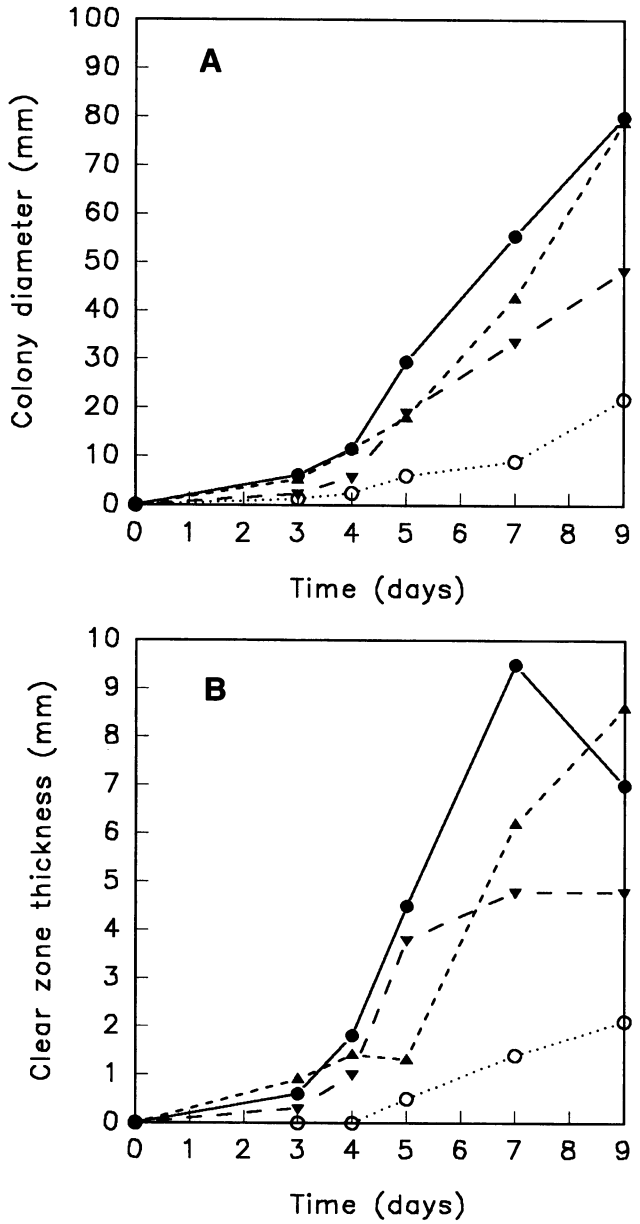

Figure 11. ABP-120$^-$ cells show a reduction in (A) the rate of colony growth and (B) clear zone width when grown on bacterial lawns. (●) 1S-2$^+$ (ABP-120$^+$), (○) 1S-4$^-$ (ABP-120$^-$), (▼) 3P-2 (ABP-120$^{-/+}$), and (▲) 5–7 (ABP-120$^{-/+}$). n = 4.

ABP-120$^-$ cells (Figures 10 and 11). However, neither of these defects was completely normalized in the rescued cells. This reduction compared with wild-type cells can be correlated to the amount of ABP-120 expressed in the rescued cell lines. In wild-type cells, in which ABP-120 is under the control of its own promotor, ABP-120 expression in cells grown on bacterial lawns is twice that of cells grown in either HL5 or bacterial suspension. The rescued cell lines did not show a similar increase in ABP-120 expression level when grown on a bacterial lawn and the level of ABP-120 expression correlated with the clear zone width. For example, colonies of rescued ABP-120$^{-/+}$ cells (3P-2) had smaller clear zones and the level of ABP-120 expression was reduced to 50.5% ± 16.3 (± SD, n = 2) that of HL5 grown cells. This lower level of expression in vegetative cells grown on bacterial lawns has been seen previously when the actin 15 promoter is used (Cohen *et al.*, 1986) and is similar to that seen with the actin 6 promoter, which also shows reduced expression when cells are grown on KA lawns (Knecht and Loomis, 1987). This point is confirmed by the ability of both ABP-120$^{-/+}$ cell lines (5–7 and 3P-2) to grow at wild-type rates in bacterial suspension, conditions under which wild-type levels of ABP-120 are expressed from the actin 15 promoter.

DISCUSSION

We originally generated ABP-120$^-$ mutants by homologous integration, and demonstrated that two independent ABP-120$^-$ cell lines exhibited very discrete defects in pseudopod extension (Cox *et al.*, 1992) and cytoskeletal structure (Cox *et al.*, 1995). However, Brink *et al.* (1990) used chemical mutagenesis to generate a cell line that did not express ABP-120, and found little difference in the behavior of their mutant and wild-type cell lines. Therefore, we were faced with apparently contradictory observations, and fundamentally opposing conclusions. Because Brink *et al.* (1990) found no obvious phenotype in their chemically generated ABP-120$^-$ cells, it could be argued that there is functional redundancy between highly similar actin binding proteins, and when one is missing, it does not really matter because another protein replaces it (Witke *et al.*, 1992). This conclusion is difficult to accept from an evolutionary point of view, because if a molecule is not necessary, there would be no evolutionary pressure for maintaining it in a functional state. That is, every actin binding protein may play a discrete role in some aspect of actin-associated function. Therefore, it seems more likely that the absence of an observed phenotype in ABP-120$^-$ cells arising from chemical mutagenesis is either the result of compensating parallel mutations, or the result of the methods used to analyze the behavioral phenotype (Condeelis *et al.*, 1993a; Soll, 1995). Chemical mutagenesis is prone to multiple mutations, and parallel mutations causing functional suppression of the consequences of a single gene mutation are not without precedent. In addition, we are becoming increasingly aware of just how complicated the process of pseudopod extension really is (Condeelis, 1993b; Wessels *et al.*, 1996; Soll, 1995), and how actin binding proteins play roles in the fine tuning of the process (Soll, 1995). It has also become increasingly clear that without high resolution methods for viewing the behavior of living cells and quantitating such basic processes as pseudopod extension (Condeelis, 1993a; Sheldon and Knecht, 1995; Soll, 1995), many of the aberrant aspects of mutant behavior can be missed.

The genesis of ABP-120$^-$ cell lines by targeted gene disruption reduces the risk of parallel mutations because one can assess the accuracy of integration by Southern analysis. The ABP-120$^-$ cell lines initially generated by targeted integration proved to contain inserts only at the ABP-120 gene locus, and two independent disruptants exhibited similar aberrant behavioral phenotypes. In addition, the ABP-120$^-$ disruptants were subjected to a far more intense computer-assisted analysis of behavior, to a more intense biochemical analysis, and to an ultrastructural analysis of the cytoskeleton (Cox *et al.*, 1992, 1995).

To demonstrate beyond a doubt that the aberrant phenotypes of ABP-120$^-$ cells, including the collapse of the actin filament network, the aberrant changes in F-actin incorporation into the cytoskeleton after cAMP stimulation, the aberrant extension of pseudopodia, and the depression in chemotactic index, are indeed specifically due to the disruption of the ABP-120 gene locus in ABP-120$^-$ cells, we have rescued an ABP-120$^-$ cell line by reintroducing ABP-120 expression. Different integration events in two rescued cell lines were verified by Southern analysis, and as demonstrated here, resulted in a return to normalcy of every measured biochemical, ultrastructural, and behavioral defect of ABP-120$^-$ cells in both cell lines. The possibility that either the original ABP-120$^-$ or the rescued ABP-120$^{-/+}$ phenotypes were due to decreased or increased expression of actin, myosin, α-actinin, or ABP-240 was ruled out, and the constancy of these cytoskeletal components in mutant and rescued cells suggests that fluctuations in other cytoskeletal elements are also unlikely.

The ABP-120$^-$ phenotype was indeed specific to the disrupted ABP-120$^-$ locus and in no way reflected either a general phenotype common to mutants of actin binding proteins or an artifact of computer-associated methods of analysis. This is best demonstrated by comparing the behavioral phenotype of ABP-120$^-$ cells with that of a number of disruptants of actin binding proteins analyzed by computer-assisted two-dimensional motion analysis systems (Soll, 1995). For instance, while ABP-120$^-$ cells form pseudopods at

one-third the frequency of wild-type cells and ABP-120$^-$ pseudopods grow to one-third the size of wild-type cells, myoA$^-$ cells form pseudopods at two times the frequency of wild-type cells and myoA$^-$ pseudopods grow to areas the same size as wild-type cells (Titus *et al.*, 1993; Wessels *et al.*, 1996). In fact, when compared with myo II$^-$ cells (Wessels *et al.*, 1989), myoA$^-$ cells (Titus *et al.*, 1993; Wessels *et al.*, 1996), myoB$^-$ cells (Wessels *et al.*, 1991), and ponticulin-minus cells (Shutt *et al.*, 1995), ABP-120$^-$ cells are the only ones that form pseudopods at a frequency lower than that of wild-type cells. These results indicate that myosin I is involved in the suppression rather than the formation of pseudopods and that cross-linking of filaments by ABP-120, not sliding of filaments by myosins, is essential for normal pseudopod extension as predicted by the Cortical Expansion Model (Condeelis, 1993b). We, therefore, conclude that the defects originally demonstrated for the ABP-120$^-$ cells produced by homologous recombination were the direct result of ABP-120 deletion.

The Function of ABP-120 in Phagocytosis

In addition, the consequences of deletion of ABP-120 on the formation of pseudopods produced during phagocytosis have been characterized. ABP-120 is localized to phagocytic cups in *Dictyostelium*. Deletion of ABP-120 results in a 50% reduction in the ability of the cells to phagocytose both latex beads and bacteria, and this correlates with the incapacity of ABP-120$^-$ cells to form normal phagocytic cups. Therefore, our results indicate that efficient phagocytosis requires normal pseudopod extension, a process that in turn requires ABP-120 (Cox *et al.*, 1992, 1995).

The decreased ability of ABP-120$^-$ cells to perform phagocytosis affects the ability of cells to grow in bacterial suspension and on bacterial lawns. Even though ABP-120$^-$ cells can grow to a limited extent by phagocytosis, growth is not as efficient as ABP-120$^+$ cells and hence ABP-120$^-$ cells would be at a marked disadvantage when placed in competition with wild-type cells in an environment where bacteria are the main food source.

Furthermore, our results indicate, as expected, that the morphology of *Dictyostelium* colonies on bacterial lawns is dependent on the ability of cells to phagocytose bacteria. Colonies of ABP-120$^-$ cells show clear defects in the rate of colony expansion and clear zone width. The defects seen in the colony morphology of ABP-120$^-$ cells can be specifically attributed to the lack of ABP-120 as shown by the rescue of the colony morphology defect upon re-expression of ABP-120 in ABP-120$^-$ cells. The increase in the rate of colony expansion and clear zone width correlates with the level of ABP-120 expression.

However, there is no difference in the ability of the cells to undergo morphogenesis, a process that is independent of the rate of phagocytosis. Therefore, use of developmental competence as a criterion for the importance of a particular protein when assessing the phenotype of a mutant can be misleading. Mutant cells should be analyzed at all stages of the life cycle for phenotypic differences. Lack of such analysis may be a contributing factor to the conclusion that deletion of various actin binding proteins results in no phenotype.

Finally, we conclude that the severity and properties of a phenotype in null cells is directly related to the properties of the deleted protein in vitro. In addition, there is no evidence for networking or compensation in the ABP-120 mutants reported here. These results indicate that the aggregate properties of the cytoskeleton are due to the sum of the activities of the individual structural proteins.

ACKNOWLEDGMENTS

The authors are grateful to the members of the Condeelis lab for editorial comments. The authors also thank the Analytical Imaging Facility at the Albert Einstein College of Medicine for the use of the confocal microscope and the National Institutes of Health for grants GM-25813 (J.C.), HL-47874 (J.H.), HD-18577 (D.R.S.), and training grant 5T32 HL-07675–03 (D.C.), which supported this study.

REFERENCES

Bray, D., and Vasiliev, J. (1989). Networks from mutants. Nature *338*, 203–204.

Brink, M., Gerisch, G., Isenberg, G., Noegel, A.A., Segall, J.E., Wallraff, E., and Schleicher, M. (1990). A *Dictyostelium* mutant lacking and F-actin cross-linking protein, the 120-kD gelation factor. J. Cell Biol. *111*, 1477–1489.

Carboni, J.M., and Condeelis, J.S. (1985). Ligand-induced changes in the location of actin, myosin, 95 K (actinin), and 120 K protein in amoebae of *Dictyostelium discoideum*. J. Cell Biol. *100*, 1884–1893.

Cohen, C.J., Bacon, R., Clarke, M., Joiner, K., and Mellman, I. (1994). *Dictyostelium discoideum* mutants with conditional defects in phagocytosis. J. Cell Biol. *126*, 955–966.

Cohen, S.M., Knecht, D., Lodish, H.F., and Loomis, W.F. (1986). DNA sequences required for expression of a *Dictyostelium* actin gene. EMBO J. *5*, 3361–3366.

Condeelis, J. (1981). Microfilament-membrane interactions in cell shape and surface architecture. In: International Cell Biology 1980–1981, ed. H.G. Schweiger, Berlin, Germany: Springer-Verlag, 306–320.

Condeelis, J. (1993a). Understanding the crawling of cells: insights from *Dictyostelium*. Trends Cell Biol. *3*, 371–376.

Condeelis, J. (1993b). Life at the leading edge: the formation of cell protrusions. Annu. Rev. Cell Biol. *9*, 411–444.

Condeelis, J., Bresnick, A., Demma, M., Dharmawardhane, S., Eddy, R., Hall, A.L., Sauterer, R., and Warren, V. (1990). Mechanisms of amoeboid chemotaxis: an evaluation of the cortical expansion model. Dev. Genet. *11*, 333–340.

Condeelis, J., Hall, A., Bresnick, A., Warren, V., Hock, R., Bennet, H., and Ogihara, S. (1988). Actin polymerization and pseudopod exten-

sion during amoeboid chemotaxis. Cell Motil. Cytoskeleton *10*, 77–90.

Condeelis, J., Vahey, M., Carboni, J.M., DeMey, J., and Ogihara, S. (1984). Properties of the 120,000- and 95,000-dalton actin binding proteins from *Dictyostelium discoideum* and their possible functions in assembling the cytoplasmic matrix. J. Cell Biol. *99*, 119s–126s.

Cox, D., Condeelis, J., Wessels, D., Soll, D., Kern, H., and Knecht, D. (1992). Targeted disruption of the ABP-120 gene leads to cells with altered motility. J. Cell Biol. *116*, 943–955.

Cox, D., Ridsdale, J.A., Condeelis, J., and Hartwig, J. (1995). Genetic deletion of ABP-120 alters the three-dimensional organization of actin filaments in *Dictyostelium* pseudopods. J. Cell Biol. *128*, 819–835.

Dharmawardhane, S., Warren, V., Hall, A.L., and Condeelis, J. (1989). Changes in the association of actin binding proteins with the actin cytoskeleton during chemotactic stimulation of *Dictyostelium discoideum*. Cell Motil. Cytoskeleton *13*, 57–63.

Dynes, J.L., and Firtel, R.A. (1989). Molecular complementation of a genetic marker in *Dictyostelium* using a genomic DNA library. Proc. Natl. Acad. Sci. USA *86*, 7966–7970.

Franke, J., and Kessin, R. (1977). A defined minimal medium for axenic strains of *Dictyostelium discoideum*. Proc. Natl. Acad. Sci. USA *74*, 2157–2161.

Fukui, Y., Lynch, T.J., Brzeska, H., and Korn, E. (1989). Myosin I is located at the leading edges of locomoting *Dictyostelium* amoebae. Nature *341*, 328–331.

Gerisch, G., Malchow, D., Huesgen, A., Nanjundiah, V., Roos, W., and Wick, J. (1975). Cyclic AMP reception and cell recognition in *Dictyostelium discoideum*. In: Developmental Biology ICN-UCLA Symposia on Molecular and Cellular Biology, vol. 2, ed. D. McMahon and C.F. Fox, Menlo Park, CA: Benjamin, 76–88.

Gerisch, G., Segall, J.E., and Wallraff, E. (1989). Isolation and behavioral analysis of mutants defective in cytoskeletal proteins. Cell Motil. Cytoskeleton *14*, 75–79.

Greenberg, S., El Khoury, J., Di Virgilio, F., Kaplan, E.M., and Silverstein, S.C. (1991). Ca^{2+}-independent F-actin assembly and disassembly during Fc receptor-mediated phagocytosis in mouse macrophages. J. Cell Biol. *113*, 757–767.

Hall, A.L., Schlein, A., and Condeelis, J. (1988). Relationship of pseudopod extension to chemotactic hormone-induced actin polymerization in amoeboid cells. J. Cell. Biochem. *37*, 285–299.

Hartwig, J., and Kwiatkowski, D. (1991). Actin binding proteins. Curr. Opin. Cell Biol. *3*, 87–97.

Hartwig, J., and Shevlin, P. (1986). The architecture of actin filaments and the ultrastructural location of actin-binding protein in the periphery of lung macrophages. J. Cell Biol. *103*, 1007–1020.

Harvath, L. (1990). Regulation of neutrophil chemotaxis: correlations with actin polymerization. Cancer Invest. *8*, 651–654.

Howard, T.H., and Oresajo, C.O. (1985). A method for quantifying F-actin in chemotactic peptide-activated neutrophils: study of the effect of tBOC peptide. Cell Motil. *5*, 545–557.

Kalpaxis, D., Werner, H., Boy-Marcotte, E., Jaquet, M., and Dingerman, T. (1990). Positive selection for *Dictyostelium* mutants lacking the uridine monophosphate synthase activity based on resistance to 5-fluoro-orotic acid. Dev. Genet. *11*, 396–402.

Knecht, D.A., Jung, J., and Matthews, L. (1990). Quantitation of transformation efficiency using a new method for clonal growth and selection of axenic *Dictyostelium* cells. Dev. Genet. *11*, 403–409.

Knecht, D.A., and Loomis, W.F. (1987). Antisense RNA inactivation of myosin heavy chain gene expression in *Dictyostelium discoideum*. Science *236*, 1081–1086.

Kraft, B., Steinbrech, D., Yang, M., and Soll, D.R. (1988). High frequency switching in *Dictyostelium*. Dev. Biol. *130*, 198–208.

Mast, S.O. (1926). Structure, movement, locomotion and stimulation in amoebae. J. Morphol. Physiol. *41*, 347–425.

Matsudaira, P. (1991). Modular organization of actin crosslinking proteins. Trends Biol. Sci. *16*, 87–92.

McCutcheon, M. (1946). Chemotaxis in leukocytes. Physiol. Rev. *26*, 401–404.

Ogihara, S., Carboni, J., and Condeelis, J. (1988). Electron microscopic localization of myosin II and ABP-120 in the cortical matrix of *Dictyostelium* amoebae using IgG-gold conjugates. Dev. Genet. *9*, 505–520.

Reaven, E.P., and Axline, S.G. (1973). Subplasmalemmal microfilaments and microtubules in resting and phagocytizing cultivated macrophages. J. Cell Biol. *59*, 12–27.

Sheetz, M., Wayne, D., and Pearlman, A. (1992). Extension of filopodia by motor-dependent actin assembly. Cell Motil. Cytoskeleton *22*, 160–169.

Sheldon, E., and Knecht, D.A. (1995). Mutants lacking myosin II cannot resist forces generated during multicellular morphogenesis. J. Cell Sci. *108*, 1105–1115.

Shutt, D.C., Wessels, D., Wagenknecht, K., Chandrasikhar, A., Hitt, A.L., Luna, E.J., and Soll, D.R. (1995). Ponticulin plays a role in the postional stabilization of pseudopods. J. Cell Biol. *131*, 1495–1506.

Soll, D.R. (1987). Methods for manipulating and investigating developmental timing in *Dictyostelium discoideum*. In: Methods in Cell Biology, vol. 28, ed. J. Spudich, San Diego, CA: Academic Press, 413–431.

Soll, D.R. (1988). "DMS", a computer-assisted system for quantitating motility, the dynamics of cytoplasmic flow and pseudopod formation: its application to *Dictyostelium* chemotaxis. In: Optical Approaches to the Dynamics of Cellular Motility, ed. J. Condeelis, Cell Motil. Cytoskeleton *10* (suppl), 91–106.

Soll, D.R. (1995). The use of computers in understanding how cells crawl. Int. Rev. Cytol. *163*, 43–104.

Soll, D.R., Voss, E., Varnum-Finney, B., and Wessels, D. (1988). The "dynamic morphology system": a method for quantitating changes in shape, pseudopod formation and motion in normal and mutant amoebae of *Dictyostelium discoideum*. J. Cell. Biochem. *37*, 177–192.

Stendahl, O., Hartwig, J., Brotschi, E., and Stossel, T. (1980). Distribution of actin-binding protein and myosin in macrophages during spreading and phagocytosis. J. Cell Biol. *84*, 215–224.

Stephens, C.C., and Snyderman, R. (1992). Cyclic nucleotides regulate the morphological alterations required for chemotaxis in monocytes. J. Immunol. *128*, 1192–1197.

Sylwester, A., Wessels, D., Anderson, S.A., Warren, R.Q., Shutt, D., Kennedy, R., and Soll, D.R. (1993). HIV-induced syncytia of a T cell line form single giant pseudopods and are motile. J. Cell Sci. *106*, 941–953.

Titus, M.A., Wessels, D., Spudich, J.A., and Soll, D. (1993). The unconventional myosin encoded by the myoA gene plays a role in *Dictyostelium* motility. Mol. Biol. Cell. *4*, 233–246.

Varnum, B., and Soll, D.R. (1984). Effects of cAMP on single cell motility in *Dictyostelium*. J. Cell Biol. *99*, 1151–1155.

Varnum-Finney, B.J., Edwards, K.B., Voss, E., and Soll, D.R. (1987). Frequency and orientation of pseudopod formation of *Dictyostelium*

discoideum amoebae chemotaxing in a spatial gradient: further evidence for a temporal mechanism. Cell Motil. Cytoskeleton *8*, 18–26.

Vogel, G., Thilo, L., Schwarz, H., and Steinhart, R. (1980). Mechanism of phagocytosis in *Dictyostelium discoideum*: phagocytosis is mediated by different recognition sites as disclosed by mutants with altered phagocytotic properties. J. Cell Biol. *86*, 456–465.

Wessels, D., Murray, J., Jung, G., Hammer, J.A., III, and Soll, D.R. (1991). Myosin IB null mutants of *Dictyostelium* exhibit abnormalities in motility. Cell Motil. Cytoskeleton *20*, 301–315.

Wessels, D., Schroeder, N., Voss, E., Hall, A., Condeelis, J., and Soll, D.R. (1989). cAMP mediated inhibition of intracellular particle movement and actin reorganization in *Dictyostelium*. J. Cell Biol. *109*, 2841–2851.

Wessels, D., Titus, M., and Soll, D.R. (1996). A *Dictyostelium* myosin I plays a crucial role in regulating the frequency of pseudopods formed on the substratum. Cell Motil. Cytoskeleton *33*, 64–79.

Witke, W., Nellen, W., and Noegel, A. (1987). Homologous recombination in the *Dictyostelium* alpha-actinin gene leads to an altered mRNA and lack of the protein. EMBO J. *6*, 4143–4148.

Witke, W., Schleicher, M., and Noegel, A.A. (1992). Redundancy in the microfilament system: abnormal development of *Dictyostelium* cells lacking two F-actin cross-linking proteins. Cell *68*, 53–62.

Wolosewick, J.J., and Condeelis, J. (1986). Fine structure of gels prepared from an actin-binding protein and actin: comparison to cytoplasmic extracts and cortical cytoplasm in amoeboid cells of *Dictyostelium discoideum*. *J. Cell Biochem. 30*, 227–243.

Zigmond, S.H. (1977). The ability of polymorphonuclear leukocytes to orient in gradient of chemotactic factors. J. Cell Biol. *101*, 1–5.

Zigmond, S.H., and Sullivan, S.J. (1979). Sensory adaptation of leukocytes to chemotactic peptide. J. Cell. Biol. *92*, 517–527.